

¹ Molecular and functional mechanisms ² of long-term visual habituation in larval ³ zebrafish

⁴ Laurie-Anne Lamiré¹, Martin Haesemeyer², Florian Engert^{3,4†},
⁵ Michael Granato^{5†}, Owen Randlett^{1†,*}

*Correspondence:

owen.randlett@

univ-lyon1.fr (OR)

⁶ Laboratoire MeLiS, UCBL - CNRS UMR52684 - Inserm U1314, Institut NeuroMyoGène, Faculté de Médecine et de Pharmacie, 8 avenue Rockefeller,

⁷ 69008, Lyon, France ; ² The Ohio State University, Department of Neuroscience, Columbus, OH 43210, USA ; ³ Department of Molecular and Cellular

⁸ Biology, Faculty of Arts and Sciences, Harvard University, Cambridge, MA 02138, USA ; ⁴ Center for Brain Science, Faculty of Arts and Sciences,

⁹ Harvard University, Cambridge, MA 02138, USA ; ⁵ Department of Cell and Developmental Biology, University of Pennsylvania, Perelman School of

[†]Equal

contribution

¹⁰ Medicine, 421 Curie Blvd, Philadelphia, PA 19104, USA

¹¹ **Abstract** Long-term habituation allows animals to learn to ignore persistent but unimportant stimuli. Despite being the most basic form of learning, a consensus model on the underlying mechanisms has yet to emerge. We have exploited a visual habituation paradigm in larval zebrafish, where larvae will learn to reduce their reactions to abrupt global dimming (a dark flash). Using a drug-screening approach, we first identified pathways that potently altered habituation learning, including GABAergic inhibition, Melatonin and Estrogen signaling. To determine how habituation manifests at the circuit-level, we used whole-brain pERK and 2-photon Ca²⁺ imaging. These analyses identified 12 classes of neurons that differ in their stimulus response profile, rate of adaptation during learning, anatomical location, and GABAergic identity. By analyzing how GABA and Melatonin alter population activity, we propose a model for dark flash habituation in which the suppression of activity begins early in the visual pathway but downstream of the retina. This suppression is mediated by GABAergic inhibitory motifs resulting in heterogeneous inhibition of distinct neuronal types in the dark flash circuit. Our results have identified multiple molecular pathways acting in functional cell types underlying a form of long-term plasticity in a vertebrate brain, and allow us to propose the first iteration of a model for how and where this learning process is encoded in individual neurons to shape learned behaviour.

²⁶ Introduction

²⁷ A central function of the brain is to change with experience: learning from the past to adapt behaviours in the now. At a base level, these adaptations can reflect attempts to identify and attend preferentially to salient stimuli. For example, identifying the smell of a predator or prey may be crucial, while identifying that my home still smells like my kin is not. This ability to suppress responses to continuous stimuli is known as habituation, and is generally considered to be the simplest form of learning and memory *Rankin et al. (2009)*. Habituation is conserved across all animals, and like other forms of plasticity, exists in at least two mechanistically distinct forms: transient short-term habituation, and protein-synthesis dependent long-term habituation. Here we focus on long-term habituation, which serves as a pragmatic model to dissect the molecular and circuit mechanisms of stably encoded plasticity processes in neural circuits.

³⁷ In recent years, a renewed focus on long-term habituation has led to significant insights into the adaptations underlying this process *Cooke and Ramaswami (2020); McDiarmid et al. (2019b)*, nonetheless a consensus model on the general principles underlying habituation is yet to emerge. Physiological and genetic work in *Aplysia*, and *C. elegans* were consistent with a model in which homosynaptic depression of excitatory synapses drives habituation *Bailey and Chen (1983); Rose et al. (2003)* (although see *Glanzman (2009)*). In contrast, recent work in the *Drosophila*

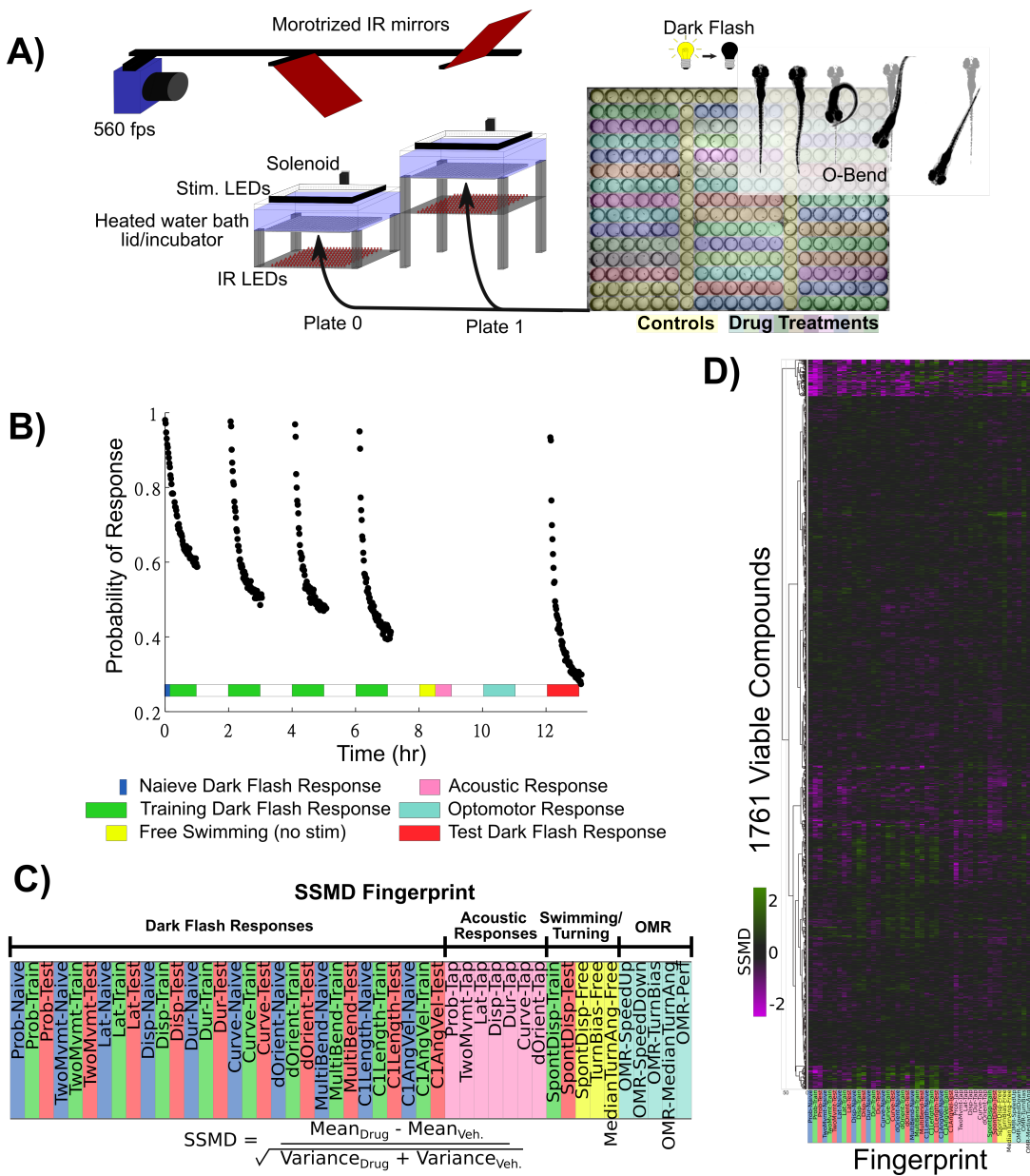


Figure 1. Pharmacological screening for dark flash habituation modulators.

A) Screening setup to record larval zebrafish behaviour in 300-well plates, which are placed below a 31°C water bath that acts as a heated lid for the behaviour plates. Two 300-well plates are imaged in alternation using mirrors mounted on stepper motors. Fish are illuminated with infra-red LEDs and imaged with a high-speed camera recording at 560 frames per second (fps). Visual stimuli are delivered by a rectangular ring of RGB LEDs, and acoustic stimuli are delivered via a solenoid mounted on the back of the water tank. Colors overlaid on the 300-well plate indicate the arrangement of small molecule treatments and controls (yellow).

B) Habituation results in a progressive decrease in responsiveness to dark flashes repeated at 1-minute intervals, delivered in 4 training blocks of 60 stimuli, separated by 1hr of rest (from 0:00-8:00). This epoch is separated into periods reflective of the Naive response (first 5 stimuli, blue), and the remaining 235 stimuli during Training (green). From 8:00-8:30, no stimuli are delivered and fish are monitored for spontaneous behaviour (yellow). From 8:30-9:00 fish are given acoustic stimuli via the solenoid tapping on the water bath (pink). From 10:00 - 11:00 fish are stimulated with alternating leftward and rightward motion using the RGB LEDs to induce the optomotor response and turning towards the direction of motion (light blue). Finally, at 12:00-13:00, larvae are given 60 additional dark flashes during the test period (red).

C) The strictly standardized mean difference (SSMD) is calculated across these different time periods, behaviours and the different components of O-Bend behavioural habituation (Randlett et al., 2019). All drugs were dosed at 10 µM in 0.1% DMSO ($n = 6$ larvae), relative to 0.1% DMSO vehicle controls ($n = 60$ larvae).

D) These vectors are assembled across all screened drugs that were viable and did not cause death or paralysis of the larvae. Displayed as a hierarchically clustered heatmap of behavioural Fingerprints (vectors of SSMD values). Clustering distance = ward, standardized euclidean.

Figure 1—source data 1. Small molecule library, Selleckchem Bioactive: 2100 FDA-approved/FDA-like small molecules

Figure 1—source data 2. Behavioural fingerprints for viable compounds

42 olfactory and gustatory systems indicate that the potentiation of inhibitory neurons drives habituation rather than
43 depression of excitatory connections *Das et al. (2011); Paranjpe et al. (2012); Trisal et al. (2022)*, and habituation to
44 specific orientations of visual cues in mice is associated with the potentiation of neuronal activity and synapses in
45 the visual cortex *Cooke et al. (2015)*, which requires GABAergic interneurons *Kaplan et al. (2016)*. These studies are
46 more consistent with a model in which the potentiation of inhibition, rather than depression of excitation, drives
47 habituation *Cooke and Ramaswami (2020)*.

48 Recently, we found that long-term habituation of the response of larval zebrafish to sudden pulses of whole-field
49 darkness, or dark flashes (DFs), involves multiple molecularly independent plasticity processes that act to suppress
50 different components of the behavioural response *Randlett et al. (2019)*. Similar behavioural, pharmacological, and
51 genetic experiments have led to comparable conclusions in acoustic short-term habituation *Nelson et al. (2022)*, and
52 habituation in *C. elegans* *McDiarmid et al. (2019a,b)*, indicating that habituation generally acts via multiple modular
53 plasticity processes. These modules act to mute or shift behavioural responses to repeated stimuli. How and where
54 these processes are implemented in the circuit, and how conserved or derived these processes are across species
55 or paradigms remains to be determined.

56 Here we have used a combination of high-throughput behavioural analyses, pharmacology and whole brain
57 imaging to propose a model of DF habituation. By combining knowledge about critical neurotransmitters derived
58 from pharmacology, with knowledge about functional classes of neurons derived from whole-brain imaging, we
59 have established a model constrained on multiple scales.

60 Results

61 Pharmacological screening strategy

62 When stimulated with a dark flash (DF), larval zebrafish execute an O-bend response. The O-bend is characterised by
63 a strong body bend and a large angle turning maneuver that forms part of the phototactic strategy of larval zebrafish,
64 helping them navigate towards lit environments *Burgess and Granato (2007); Chen and Engert (2014)*. When trained
65 with repeated DFs, larvae will habituate and reduce their responsiveness in multiple independent ways, includ-
66 ing: decreasing response probability, increasing latency, and decreasing multiple measures of response magnitude
67 *Randlett et al. (2019)*. As the molecular mechanisms leading to this form of habituation learning are still largely
68 unknown, we used a pharmacological screening approach with the goal of identifying important molecular players
69 in habituation. We used the high-throughput assay we previously established, which has a maximum throughput
70 of 600 larvae/day (*Figure 1A, Randlett et al. (2019)*). As we aimed to identify modulators specific for habituation,
71 we included additional behavioural assays as controls, including the response to acoustic stimuli, the optomotor
72 response, and the spontaneous swimming behaviour of the fish in the absence of stimulation (*Figure 1B,C*).

73 Behavioural records for fish treated with each compound were compressed into a fingerprint *Rihel et al. (2010)*
74 – a vector representing the strictly standardised mean difference (SSMD) across 47 aspects of behaviour (see Meth-
75 ods). For measurements related to dark-flash habituation behaviour, responses were time-averaged across three
76 epochs chosen to highlight changes in habituation: the naive response (first 5 dark flashes), the response during the
77 remaining training flashes, and the re-test block 5 hrs after training (*Figure 1B*). This was done across 10 different
78 components of the dark flash response (Probability of Response, Latency, Displacement, etc.).

79 In each 300-well plate, 40 groups of 6 larvae were treated in individual wells, and compared to 60 vehicle treated
80 controls (*Figure 1A*). We chose these numbers based on a sub-sampling analysis that determined these numbers
81 were sufficient to identify the effect of a known modulator of habituation (haloperidol *Randlett et al. (2019)*) at a
82 false-negative rate of less than 0.05 (not shown), while allowing us to screen 80 drugs per experiment across 2 plates
83 (*Figure 1A*).

84 Correlational structure in the pharmaco-behavioural space

85 We screened a total of 1953 small molecule compounds for their acute effects on behaviour (*Figure 1-source data 1*)),
86 focusing on both activators and inhibitors with annotated targets. We were able to collect the full behavioural
87 record of 1761 compounds (*Figure 1D, Figure 1-source data 2*)), indicating that the fish survived the treatment
88 and maintained their ability to swim. We found that 176 drugs significantly altered at least one aspect of measured
89 behaviour, yielding a 9% hit rate (hit threshold of $|SSMD| \geq 2$). While the average effect was to suppress behavioural

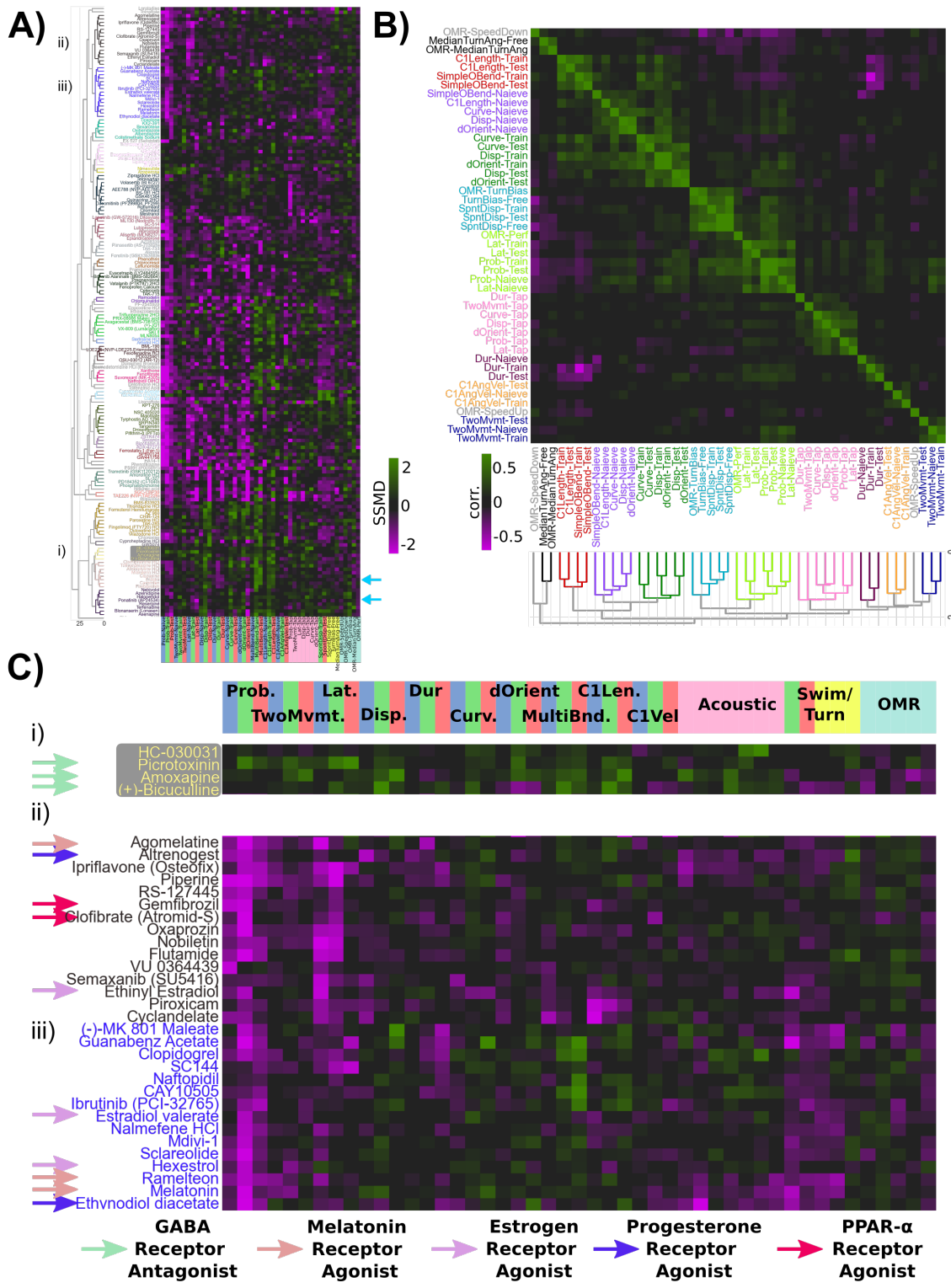


Figure 2. Pharmaco-behavioural analyses of behaviour-modifying compounds.

A) Clustered heatmap of the behavioural Fingerprints for the 176 hits of the screen, showing at least one behaviour measure with $|SSMD| \geq 2$. Clustering distance = ward, standardized euclidean. This led to the re-identification of Haloperidol and Clozapine as habituation modifiers (light blue arrows).

B) Clustered correlogram of the Pearson correlation coefficients for the different measured components of behaviour across hits (same data as (A)) revealing the independence or co-modulation of behaviours. Clustering distance = average, correlation.

C) Subsets of clustered heatmap from (A), highlighting the similar phenotypes exhibited by i) GABA Receptor antagonists and ii), iii) Melatonin receptor agonists, Estrogen receptor agonists, Progesterone receptor agonists and peroxisome proliferator-activated receptor alpha (PPAR α) agonists.

90 output ($SSMD = -0.20$), which could reflect non-specific toxicity or a generalized inhibition of motor output, the
91 effect of most small molecules induced both positive and negative changes in behavioural output, indicating that
92 toxicity is not the primary phenotypic driver (*Figure 2A*). While the false negative rate is difficult to determine since
93 so little is known about the pharmacology of our system, we note that of the three small molecules we previously
94 established to alter dark flash habituation that were included in the screen (Clozapine, Haloperidol and Pimozide),
95 two were identified among our hits.

96 To explore the pharmaco-behavioural space in our dataset we clustered small molecules based on their be-
97 havioural phenotypes (*Figure 2A*). This strategy can identify drugs that share common pharmacological targets, or
98 perhaps distinct pharmacological targets that result in convergent behavioural effects *Bruni et al. (2016); Rihel et al.*
99 (*2010*). Indeed, drugs known to target the same molecular pathways often showed similar behavioural fingerprints
100 lying proximal on the linkage tree, indicating that our dataset contains sufficient signal-to-noise to recover consistent
101 pharmaco-behaviour relationships.

102 Alternatively, drugs can be considered as tools to manipulate different aspects of brain function agnostic to their
103 molecular mechanisms. Consequently, using similarities and differences among the induced alterations should
104 uncover molecular and neural linkages among different behavioural outputs. Following this logic, the ability of a
105 drug to co-modify different aspects of behaviour would reflect molecular and/or circuit-level dependencies. For
106 example, visual behaviours that all depend upon the retinal photoreceptors should be similarly affected by any
107 drugs that modulate phototransduction in these photoreceptors. We quantified these relationships by calculating
108 the correlated effects on our different behavioural measurements across drugs (*Figure 2B*).

109 Consistent with our previous results highlighting uncorrelated learning across the behavioural components of
110 the O-bend response during habituation *Randlett et al. (2019)*, we found that different aspects of the response
111 were independently affected pharmacologically, resulting in distinctive correlated groupings within the correlogram.
112 While we previously found that O-Bend response Probability and Latency habituate independently in individual fish
113 *Randlett et al. (2019)*, in our drug screen data these appear to be tightly coupled (*Figure 2B*, green cluster). This may
114 result from their reliance on a common molecular-level mechanism that occurs in distinct circuit loci. However, the
115 performance of the animals in the OMR assay under different treatments was also associated with O-bend Probabil-
116 ity and Latency, suggesting that pharmacological modulation of general visual acuity could drive these correlations
117 within the drug screen dataset.

118 These analyses confirm habituation behaviour manifests from multiple distinct molecular mechanisms that in-
119 dependently modulate different behavioural outputs. Our screen was successful in identifying small molecules that
120 differentially modulate these distinct aspects of habituation behaviour, as well as acoustic, optomotor, and sponta-
121 neous behaviour.

122 Molecular pathways implicated in habituation

123 For the remainder of the analyses we chose to focus on the mechanisms leading to the habituation of response
124 probability, as this is the criterion for which it is easiest to identify the link between neural activity and behavior,
125 providing the best entry point for studying the circuit mechanisms of long-term habituation. To identify the most
126 promising hits, we sought to identify drugs that:

- 127 1. Have minimal effects on the naive response to DFs, but strong effects during the training and/or memory-
128 retention periods. This would prioritize pathways that affect habituation, rather than simply DF responsive-
129 ness.
- 130 2. Have minimal effects on other aspects of behaviour. We purposefully assayed additional behaviours after
131 habituation training in order to exclude compounds that would alter generalized arousal, movement abil-
132 ity/paralysis, or visual impairment. Such drugs would strongly influence DF responsiveness, but likely inde-
133 pendently of pathways related to habituation.
- 134 3. Show similar behavioural effects to other drugs screened that target the same molecular pathway. Such rela-
135 tionships can be used to cross validate, yet we note that our library choice was very broad, and target coverage
136 is non-uniform. Therefore a lack of multiple hits targeting the same pathway should not necessarily be taken
137 as strong evidence of a false positive.

138 This prioritization led us first to the identification of the GABA_{A/C} Receptor antagonists Bicuculline, Amoxapine,

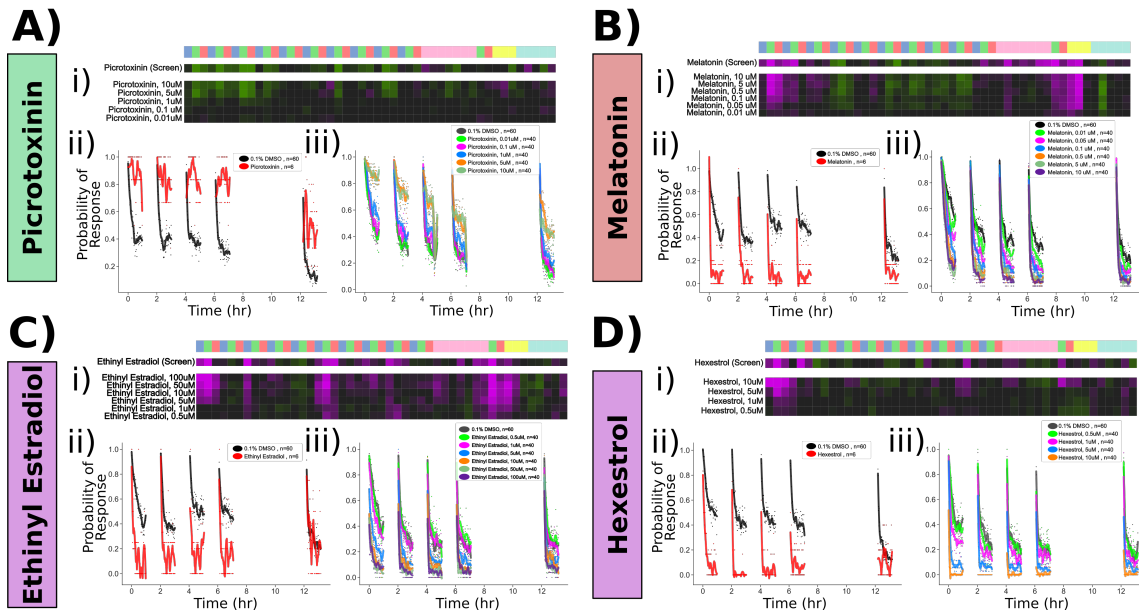


Figure 3. Confirmed pharmacological modulators of habituation.

Dose response studies for **A) Picrotoxinin**, **B) Melatonin**, **C) Ethynodiol Estradiol** and **D) Hexestrol**.

Displayed for each treatment are: i) Behavioural fingerprint for the original screen data ($10\text{ }\mu\text{M}$), and the dose response data. ii) Original screen data for the probability of response to DF stimuli. Each dot is the probability of response to one flash. Lines are smoothed in time with a Savgolay Filter (window = 15 stimuli, order=2). iii) Dose response data for the probability of response, plotted as in ii)

Figure 3—figure supplement 1. Pharmacological manipulation of control behaviours and response displacement during habituation

and Picrotoxinin (PTX). PTX treatment had the strongest effects, with increased responsiveness to DFs during the training and test periods, indicative of defects in habituation (**Figure 2Ci**). Dose-response experiments confirmed a strong effect of PTX on inhibiting the progressive decrease in responsiveness during habituation learning at $1\text{--}10\text{ }\mu\text{M}$ doses. Importantly, like the naive dark-flash response, the acoustic and optomotor response were not inhibited (**Figure 3A**, **Figure 3—figure Supplement 11A**). While strong $\text{GABA}_{\text{A/C}}$ R inhibition will result in epileptic activity in larval zebrafish, we did not observe evidence of seizure-like behaviour at these doses, consistent with previous results *Bandara et al. (2020)*. Therefore, we conclude that partial antagonism of GABA_{A} R and/or GABA_{C} R is sufficient to strongly suppress habituation, indicating that GABA plays a very prominent role in habituation resulting in this strong sensitivity to manipulation. This is consistent with a model in which the potentiation of inhibition actively silences sensory-induced activity during habituation to suppress motor output, rather than the depression of excitatory neurotransmission in the activated pathway *Cooke and Ramaswami (2020); Ramaswami (2014)*.

We next turned our attention to the upper portion of the clustered behavioural fingerprint graph (**Figure 2A**), where strong and relatively specific inhibition of responsiveness during training and testing were observed, indicative of enhanced habituation (**Figure 2Cii, iii**). Among the hits observed here were multiple agonists of both Melatonin and Estrogen receptors, indicating that neuro-hormonal signaling may play a prominent role in plasticity underlying habituation. Dose response studies with Melatonin confirmed strong potentiation of habituation (**Figure 3B**). Melatonin did cause a decrease in spontaneous movement behaviour, consistent with its role in arousal/sleep regulation in zebrafish and other vertebrates *Gandhi et al. (2015); Zhdanova et al. (2001)*, yet Melatonin did not inhibit the naive response to dark flashes, the responsiveness to acoustic stimuli or OMR performance (**Figure 3B, Figure 3—figure Supplement 11A**), indicating it does not cause generalized sedation but modulates specific aspects of behaviour at these doses, including increasing habituation.

We similarly validated that the Estrogen Receptor agonists Ethynodiol Estradiol and Hexestrol, potentiated habituation at $5\text{--}100\text{ }\mu\text{M}$ and $1\text{--}10\text{ }\mu\text{M}$ doses, respectively (**Figure 3C,D**). However, Ethynodiol Estradiol strongly suppressed movement rates at these doses, and both treatments suppressed acoustic responsiveness and OMR performance

163 at doses $\geq 10\mu M$ (*figure Supplement 11C,D*). Therefore, it is less clear how specific or generalized Estrogen Recep-
164 tor agonism is on behaviour, although the effective doses of Hexestrol for influencing habituation (1-5 μM) were
165 lower than those that significantly affected other behaviours (10 μM). Nevertheless we decided to focus on PTX and
166 Melatonin for the remaining experiments.

167 Our screening approach has identified both expected (GABA) and unexpected (Melatonin, Estrogen) pathways
168 that strongly modulate habituation of responsiveness. We have also implicated multiple additional pathways in
169 habituation, including Progesterone and PPAR α (*Figure 2C*), as well as OMR, acoustic and spontaneous behaviour,
170 which can be mined for future projects investigating the molecular basis of behaviour.

171 **Dark flash-induced neural activity is broadly inhibited during habituation**

172 Having identified molecular components of habituation, we next aimed to identify how these molecules act within
173 the circuit to modify neural activity and subsequent behavioural output. For this we used the MAP-Mapping strat-
174 egy, which allows us to measure whole-brain activity patterns from freely-swimming larvae based on their relative
175 levels of pERK immunostaining *Randlett et al. (2015)*. MAP-Mapping yields a picture of the activity patterns in the
176 experimental setting that is closest to the drug-screen situation. We determined which areas of the brain respond
177 to DFs by comparing the pERK patterns in larvae stimulated with 10 DFs at 1 min intervals, to those that were not
178 stimulated (*Figure 4B, M*). These larvae were treated with 0.1% DMSO as a vehicle control for the pharmacological
179 experiments (below). This revealed widespread activation of the brain in response to DFs, including visual areas
180 such as the retina (ret), tectum (tec), pineal, petecum and thalamus, indicating that a distributed sensory circuit is
181 activated by DFs. However, relatively little signal was observed in the telencephalon or the habenula, indicating that
182 these structures are not central to the DF response. Strong activation was seen in the hindbrain and cerebellum,
183 likely reflecting motor-related signals related to the O-bend response.

184 We then asked how this pattern changes as the animals learn. We focused on a single training block of 60
185 DFs, as this is the period under which the strongest learning takes place, and where our chosen pharmacological
186 treatments have the strongest effects relative to controls (*Figure 3*). Since the pERK indicator integrates over the
187 last ≈ 15 minutes of life, but is biased towards the terminal 5 minutes *Randlett et al. (2015)*, these experiments were
188 designed to highlight the final DFs after learning has taken place.

189 Indeed, these larvae showed much weaker activation across most of the brain (*Figure 4C, M*), which resulted in
190 widespread decreases in neural activity compared to the 10 DF group (*Figure 4D, M*). This indicates that the plasticity
191 underlying habituation affects neurons relatively early in the visual pathway, resulting in depressed activation in pri-
192 mary sensory areas (e.g. tectum and pretectum), as well as motor-related areas presumed to lie more downstream
193 in the sensory-motor circuit (e.g. tegmentum and hindbrain). However, the retina was not depressed, indicating
194 that habituation occurs downstream of this sensory ganglion.

195 To test our model of early visual pathway plasticity, we asked if the inhibition of habituation (via GABA_{A/C}R inhibi-
196 tion using PTX), or its potentiation (via Melatonin), led to the expected alterations in MAP-Maps. We first determined
197 that Melatonin alone failed to strongly alter neural activity (*Figure 4E, M*), while PTX induced the expected activation
198 associated with GABA inhibition, most prominently in the telencephalon (*Figure 4I,M*). Surprisingly, the naive re-
199 sponse to DFs was potentiated in the Melatonin treatment and suppressed in the PTX treatment relative to their
200 baseline activity, indicating that alterations in naive visual acuity for DFs is insufficient to explain the habituation
201 phenotypes associated with these treatments (*Figure 4F,J,M*). Finally, when assaying for the depression of activity
202 in trained fish relative to their naive response to DFs, we found that Melatonin treatment did indeed increase the
203 observed depression, while PTX inhibited this depression, including in primary visual areas proximal to the retinal
204 arborisation fields, the thalamus, pretectum, hypothalamus, and tectum neuropil (*Figure 4G,H,K-N*).

205 These whole-brain functional activity surveys demonstrate that habituation learning is associated with a surpris-
206 ingly strong depression of neural activity, considering that at the behavioural level larvae remain quite responsive
207 to DF stimuli after only one training block (Figure 1-3). These apparent discrepancies may reflect the presumably
208 complex and non-linear relationship between neural activity and pERK responsiveness. Combined with the phar-
209 macological manipulations, these experiments support a model in which habituation plasticity begins early in the
210 visual pathway. However, the temporal and spatial resolution of these experiments is insufficient to differentiate
211 how individual neurons adapt during habituation, and therefore do not exclude the possibility that habituation oc-
212 curs within the the retina, perhaps at the retinal ganglion cell terminals, where the central brain would simply receive

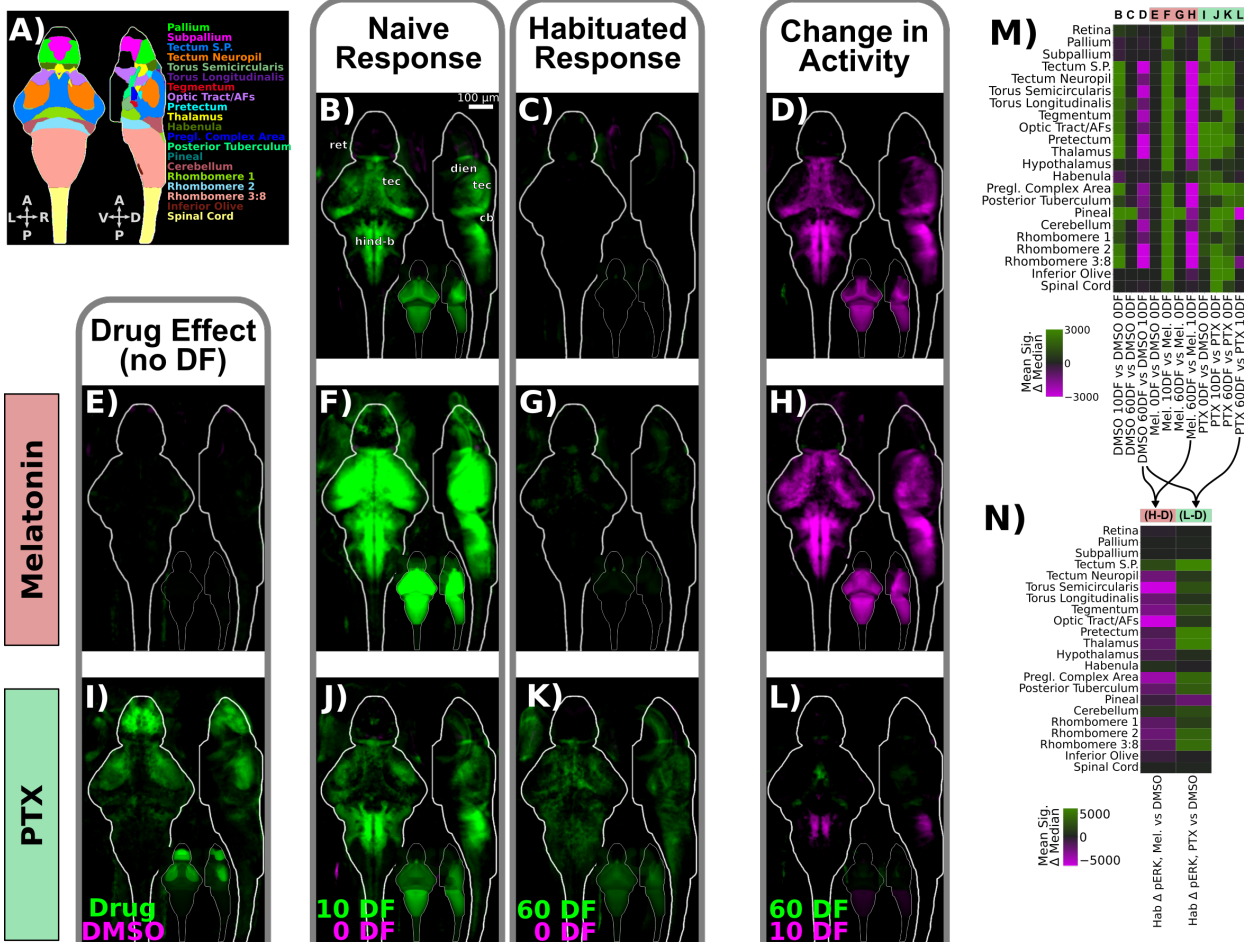


Figure 4. pERK-based whole-brain mapping of altered neural activity during habituation

A) Anatomical regions in the Z-Brain coordinate space used for image display and analyses. A = anterior, P = posterior, L = left, R = right, V = ventral, D = dorsal.

B-L) MAP-Maps showing areas with whole-brain differences in pERK/tERK staining intensity, with green and magenta representing significantly increased staining in the relevant group in the pairwise comparison. Shown as summed intensity projections in the Z-Brain coordinate space in the dorso-ventral (left) and sagittal (right) dimensions. Lower inset represents the average signal binned by brain regions. MAP-Maps were calculated for pairwise differences between the following treatments in: Column 1: "Drug Effect (no DF)" = drug treatment with no stimulation (green) vs. DMSO with no DFs (magenta) Column 2: "Naive Response" = Response to 10 DFs (green) vs. 0 DFs (magenta) Column 3: "Habituated Response" = Response to 60 DFs (green) vs. 0 DFs (magenta) Column 4: "Change in Activity" = Response to 60 DFs (green) vs. 10 DFs (magenta). Pharmacological treatments arranged in rows as: Row 1 0.1% DMSO, 0 DF = 26; Row 2 Melatonin, 0.1 μ M in 0.1% DMSO, 0 DF = 29; Row 3 Picrotoxinin (PTX), 5 μ M in 0.1% DMSO, 0 DF = 28; Row 4 Picrotoxinin, 10 DF = 23; Row 5 Picrotoxinin, 60 DF = 27. DF = Dark Flash, Mel = Melatonin, PTX = Picrotoxinin.

M) Mean signal in brain regions for each of the experiments shown in A-K, shown as a vector in the heatmap. Same data as insets in A-K

N) Difference in the MAP-Map signals in brain areas comparing drug treated fish to DMSO control when stimulated with 60 DF vs 10 DF. Resultant differences reflect altered activity during habituation training by the drug treatment. Number of imaged fish per experimental group were: 0.1% DMSO, 0 DF = 26; 0.1% DMSO, 10 DF = 29; 0.1% DMSO, 60 DF = 23; Melatonin, 0 DF = 29; Melatonin, 10 DF = 23; Melatonin, 60 DF = 19; Picrotoxinin, 0 DF = 28; Picrotoxinin, 10 DF = 23; Picrotoxinin, 60 DF = 27. DF = Dark Flash, Mel = Melatonin, PTX = Picrotoxinin.

213 an increasingly depressed signal from the periphery.

214 **Volumetric 2-photon Ca²⁺ imaging of habituation learning**

215 Having identified the regional alterations in activity associated with habituation learning, we next asked how the
216 properties of individual neurons within the DF responsive circuit adapt during habituation. We used a head-fixed
217 paradigm to perform 2-photon Ca²⁺ imaging during habituation learning. We expressed nuclear-targeted GCaMP7f
218 pan-neuronally and imaged with a resonant scanner and piezo objective, enabling us to cover a volume of $\approx 600 \times$
219 $300 \times 120 \mu\text{m}$ (x,y,z) sampled at $0.6 \times 0.6 \times 10 \mu\text{m}$ resolution, leading to the detection of 30890 ± 3235 ROIs per larvae
220 ($\pm \text{SD}$, *Figure 5A,C*). ROIs were aligned to the Z-Brain atlas coordinates *Randlett et al. (2015)*, demonstrating that this
221 volume spans most of the areas implicated in DF habituation by our MAP-Mapping experiments (*Figure 4*), including
222 the majority of the midbrain, hindbrain, pretectum and thalamus (*Figure 5A-C*). Visual stimuli were delivered via a red
223 LED, and larvae were stimulated with 60 DFs at 1 min intervals to induce habituation learning. This induced strong
224 Ca²⁺ activity in neurons (*Figure 5C*), some of which were clearly associated with the DF stimuli. Ca²⁺ transients in
225 response to DFs generally decreased across the 60 stimuli, though this pattern was not seen in all neurons, and
226 substantial heterogeneity in their adaptations were observed. Strong correlated patterns were also seen in large
227 groupings of neurons, predominantly in the hindbrain, which were associated with movement events through their
228 correlation with motion artifacts in the imaging data (*Figure 5-figure Supplement 1*).

229 To explore the spatial patterns in these datasets we used a 2-dimensional lookup table to simultaneously visu-
230 alize the correlation and bias of Ca²⁺ fluctuations with regressors representing either DF stimuli or movement (*Fig-*
231 *ure 5E, F*). This revealed segregated populations of neurons coding for the DFs (pink) and movement (green/teal).
232 Similar patterns are visible in individuals and across the entire population of 34 larvae. As expected, DF-tuned neu-
233 rons were located predominantly in visual sensory areas in the midbrain (tectum) and diencephalon (pretectum
234 and thalamus). Motor-coding neurons dominated in the hindbrain, with the exception of the cerebellum and infe-
235 rior olive, which was predominantly tuned to the sensory stimulus. Some neurons did show approximately equal
236 correlation values to both stimuli, as evidenced by the blue-ish hues. Finally, some areas of the brain appeared to
237 contain mixtures of neurons with different coding properties, including the ventral diencephalon and midbrain.

238 To determine if there was any spatial logic to how different neurons adapt their responsiveness to DFs during
239 imaging we plotted the ROIs using a lookup table highlighting the preference of ROIs for either the first three DFs
240 (pink, naive response), or last three DFs (green, trained response). Strong preferences for the naive stimulus reflects
241 a depressing response profile (*Figure 5G, H*). Indeed, most neurons did show tunings consistent with strong depres-
242 sion, however there were neurons who showed an equal preference for naive and trained stimuli, or even stronger
243 preference for the latter, indicating stable or potentiating response profiles. These non-depressing neurons were
244 mostly contained in the dorsal regions of the brain, including the torus longitudinalis, cerebellum and dorsal hind-
245 brain. These results demonstrate that while the majority of neurons across the brain depress their responsiveness
246 during habituation, a smaller population of neurons exists that show the opposite pattern.

247 From these experiments we conclude that habituation does not occur exclusively within the retina, as in such
248 a model neurons that show stable responses or that potentiate would not be present in the brain. Instead, these
249 data are consistent with the model arising from our pERK analysis, where habituation begins early within the vi-
250 sual pathway, but downstream of the retina. However, the fact that non-depressing neurons are observed within
251 structures like the caudal hindbrain and the cerebellum indicates that even in motor-related brain regions contain
252 non-depressed signals, and thus plasticity could also be occurring in regions very downstream in the visual sensory-
253 motor pathway.

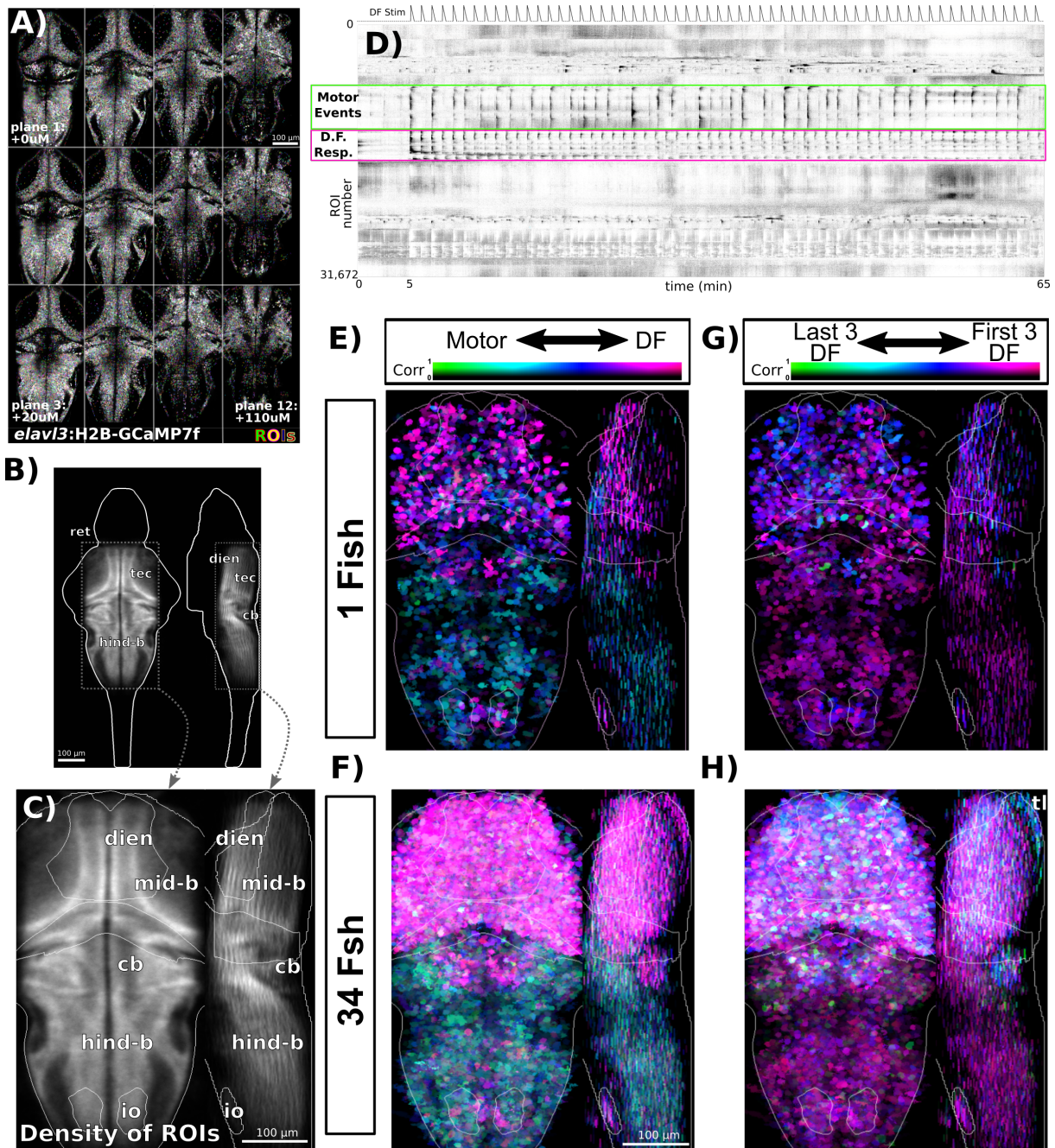


Figure 5. Volumetric 2-photon Ca^{2+} imaging of dark flash habituation.

A) *Tg(elavl3:H2B-GCaMP7f)* larvae were imaged across 12 z-planes at $10\mu\text{m}$ steps. ROIs segmented using suite2p **Pachitariu et al. (2017)** are overlaid in random colors.

B) Density of detected ROIs registered and plotted in the Z-Brain coordinate space. $n=1,050,273$ ROIs across 34 larvae.

C) Cropped field of view used for plotting and analyzing Ca^{2+} imaging data and approximate anatomical localizations of major brain areas: dien=diencephalon, mid-b = midbrain, cb = cerebellum, hind-b = hindbrain, io = inferior olive, ret = retina, tec = tectum

D) Functional responses of the population of neurons in the same fish as A), plotted as a clustered heatmap ("rastermap" **Pachitariu et al. (2017)**, github.com/MouseLand/rastermap), where rows represent individual neurons ordered by the similarities in their activity. Darker shades reflect increased activity. This clustering reveals neurons that are tuned to the DF stimuli (pink box) or motor events (green box). Dashed trace above the heatmap depicts the DF stimulus convolved with a kernel approximating H2B-GCaMP7f kinetics.

E) ROIs in an individual fish plotted based on their correlation and tuning to regressors defining either Motor or DF stimulus events, highlighting the spatial distributions of these tunings across the imaged population. Plotted as a maximum intensity projection.

F) Same analysis as E, but across the entire population of 34 larvae.

G) ROIs in an individual fish plotted based on their correlation and tuning to regressors defining either the first or last three DF stimuli.

H) Same analysis as G, but across the entire population of 34 larvae. tl = torus longitudinalis

Figure 5—figure supplement 1. Validation of motion analysis based on image artifacts during 2-photon imaging

254 **Functional classification and anatomical localization of neuronal types observed during habituation learning**

255 To categorize the functional heterogeneity within the DF-tuned neurons we used affinity propagation clustering.
256 This method has the advantage that cluster number does not need to be defined beforehand, and attempts to
257 identify the most representative response profiles algorithmically *Förster et al. (2020)*. This identified 12 clusters
258 that differed both in their adaptation to repeated DFs, as well as the shape of their response to the DF (*Figure 6A,B*).
259 We therefore use these two dimensions of the response to label the clusters:

260 Adaptation Profile: (Depression vs. Potentiation)

261 **No Adaptation** = noA : Cluster 1, 9, 10

262 **Weak Depression** = weakD : Cluster 5, 6, 11

263 **Medium Depression** = medD : Cluster 2, 3, 7

264 **Strong Depression** = strgD : Cluster 4, 8

265 **Potentiation** = Pot : Cluster 12

266 Response Shape: (Transient/Short vs. Sustained/Long)

267 **On-response** = $_{On}$: Cluster 1, 2

268 **Long/sustained response** = $_{L}$: Cluster 3, 4

269 **Medium-length response** = $_{M}$: Cluster 5, 6, 9

270 **Short/transient response** = $_{S}$: Cluster 7, 8, 10, 11

271 Yielding clusters: $^{noA}_{On}$, $^{medD}_{On}$, $^{medD}_L$, $^{strgD}_L$, $^{weakD}_M$, $^{weakD}_M$, $^{medD}_S$, $^{strgD}_S$, $^{noA}_M$, $^{noA}_S$, $^{weakD}_S$, and $^{Pot}_M$

272 While these results indicate the presence of a dozen functionally distinct neuron types, such cluster-based analyses
273 will force categories upon the data irrespective of if such categories actually exist. To determine if our cluster anal-
274 yses identified genuine neuron types, we analyzed their anatomical localization (*Figure 6C, D*). Since our clustering
275 was based purely on functional responses, we reasoned that anatomical segregation of these clusters would be
276 consistent with the presence of truly distinct types of neurons. Indeed, we observed considerable heterogeneity
277 both within and across brain regions. For example: $^{weakD}_S$ was mostly restricted to medial positions within the optic
278 tectum; $^{medD}_L$ and $^{strgD}_L$ were more prevalent within motor-related regions of the brain including the Tegmentum
279 and Hindbrain Rhombomeres; $^{noA}_M$ was the most prominent cluster in the torus longitudinalis, consistent with the
280 presence of non-depressing signals in the area (*Figure 5G,H*).

281 We then quantified the similarity in the spatial relationships among the clusters by looking at the correlations in
282 the positions of the ROIs in downsampled super-voxels of the Z-Brain (*Figure 6E*). This revealed similar hierarchical
283 relationships to those identified functionally (*Figure 6B*), especially with respect to *Response Shape*, indicating that
284 physical proximity is predictive of the functional similarity of neurons, even across clusters.

285 Finally, since our functional analysis was performed purely based on correlations with the DF stimuli, we asked to
286 what extent neurons belonging to each cluster were correlated with motor output. This identified $^{strgD}_L$ as the most
287 strongly correlated to motor output, consistent with its strong habituation profile and its localization within motor-
288 regions of the hindbrain. This indicates that $^{strgD}_L$ neurons likely occupy the most downstream positions within the
289 sensory-motor network.

290 These results highlight a diversity of functional neuronal classes observed during DF habituation. Whether there
291 are indeed 12 classes of neurons, or if this is an over- or under-estimate, awaits a full molecular characteriza-
292 tion. However, we proceed under the hypothesis that these clusters define neurons that play distinct roles in the DF
293 response and/or its modulation during habituation learning.

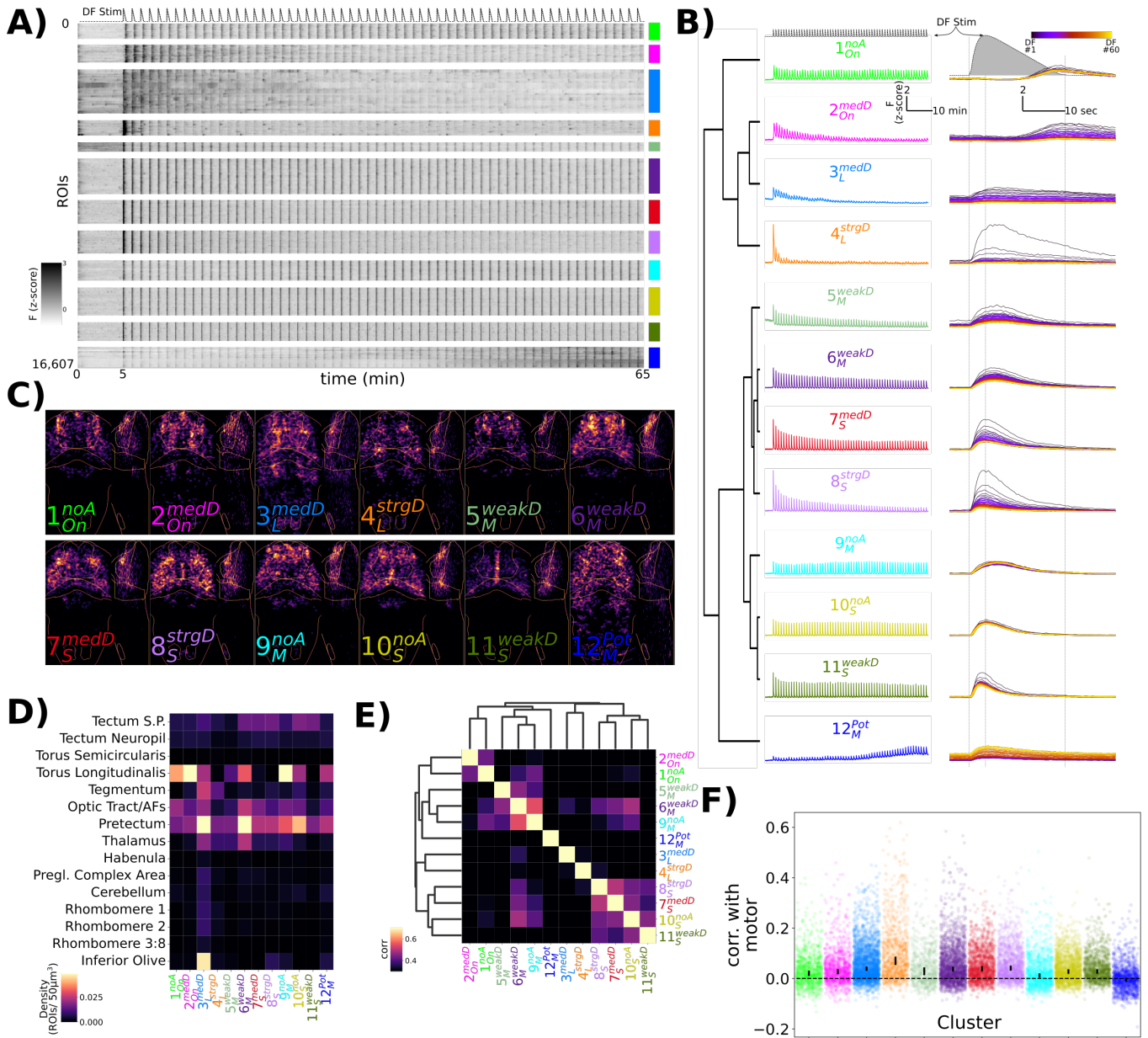


Figure 6. Characterization of functional response types during habituation learning.

- A)** Heatmap of the response profiles of ROIs categorized into 12 functional clusters. n=16,607 ROIs from 34 larvae.
- B)** Average z-scored fluorescence each functional cluster plotted for the whole experiment (left column), and centered on each DF stimulus (right column), demonstrating the differences in both *Adaptation Profiles* and *Response Shape* for each cluster. Clusters were identified using Affinity Propagation clustering (affinity = Pearson correlation, damping = 0.9, preference = -9), and organized using Hierarchical clustering, distance = complete, correlation. Dashed lines in top panels are the DF stimulus convolved with a kernel approximating H2B-GCaMP7f kinetics, used as the regressor in the analysis.
- C)** Summed intensity projection of the ROIs belonging to each functional cluster in Z-Brain coordinate space depicting their physical locations in the brain. Projection images are normalized to the maximum value.
- D)** Heatmap depicting the density of each cluster that is found within different Z-Brain regions.
- E)** Correlogram calculated from the Pearson correlation in downsampled volumes for the ROI centroid positions for each cluster (see Methods). Hierarchical clustering, distance = complete, correlation.
- F)** Correlation between motor events and the Ca²⁺ traces for each ROI assigned to the functional clusters. dots = individual ROIs, bar height = 99.9999% confidence interval around the median value.

295 **Identification of GABAergic inhibitory neurons during habituation**

296 How might the functional classes of neurons we identified interact within a circuit to drive habituation behaviour?
297 Considering that we have implicated GABAergic inhibition in habituation, the simplest model would assign a GABAergic
298 identity to the potentiating neurons; 12_M^{Pot} . These inhibitory neurons would then act to progressively increase in-
299 hibition during learning (*Figure 7A, Model 1*). Potentiation of these neurons could be achieved through, for example,
300 LTP at their inputs during learning.

301 A limitation of the pan-neuronally expressed GCaMP imaging approach is the lack of knowledge as to the molec-
302 ular identity of neurons, such as neurotransmitter type. Virtual co-localization analyses with 3D atlases can be used
303 to identify candidate molecular markers for functionally identified neurons, provided sufficient stereotypy exists in
304 neuronal positioning, and the relevant marker exists in the atlas *Dunn et al. (2016); Randlett et al. (2015)*. Therefore,
305 we analyzed the spatial correlations for markers contained in the Z-Brain *Randlett et al. (2015)*, Zebrafish Brain
306 Browser *Gupta et al. (2018); Marquart et al. (2017); Tabor et al. (2018)*, and mapZebrain atlases *Kunst et al. (2018);*
307 *Shainer et al. (2022)*. We identified markers showing the highest spatial correlations with any of our functional
308 clusters (corr. > 0.15, n=89 of 752 markers), and organized these hierarchically (*Figure 7B*).

309 We were particularly interested in associations with GABAergic neurons labeled by the *gad1b* reporter lines.
310 These were located in a region of the hierarchy showing greatest spatial similarity with 10_S^{noA} and 11_S^{weakD} (*Figure 7C*).
311 An enrichment along the medial tectum is common to markers in this region of the hierarchy, where the highest
312 density of GABAergic neurons within the tectum reside. Contrary to *Model 1*, 12_M^{Pot} neurons did not appear to be
313 associated with GABAergic neuronal markers in this analysis.

314 These data indicated that 10_S^{noA} and 11_S^{weakD} neurons are the predominant GABAergic classes. To test this, we
315 imaged the response of neurons in *Tg(Gad1b:DsRed);Tg(elavl3:H2B-GCaMP6s)* double transgenic larvae, and classified
316 neurons as *gad1b*-positive or -negative based on DsRed/GCaMP levels (*Figure 7D*). Indeed we saw a heterogeneous
317 distribution of *gad1b*-positive neurons across functional clusters, including a significant enrichment in not only 10_S^{noA}
318 and 11_S^{weakD} , but also the other two clusters with the "Short" Response Shape (7_S^{medD} and 8_S^{strgD} , *Figure 7E*). The remaining
319 clusters either showed no significant bias, indicating that they contain mixed populations, or a significant depletion
320 of *gad1b*-positive cells, suggesting that they comprise mostly of excitatory or neuromodulatory neurons (3_L^{medD} and
321 12_M^{Pot}).

322 Therefore, these results are inconsistent with *Model 1*, since 12_M^{Pot} neurons appear to be mainly non-GABAergic.
323 Instead, GABAergic neurons span the remainder of the range of adaptation profiles, from non-adapting to strong-
324 depression. These neurons are best characterized by the shape of their response to the stimulus, perhaps reflecting
325 a transient bursting style of activity relative to other neuronal types that exhibit more sustained firing patterns.

326 **A pharmacologically-constrained model of the habituating circuit**

327 Our functional and anatomical analyses indicate that distinct populations of GABAergic neurons exist that inhibit
328 behavioural responsiveness during learning. What connectivity and plasticity mechanisms might underlie the rela-
329 tionships between these neurons, and how do they shape the functional patterns of other neurons in the circuit?
330 We currently do not have sufficient anatomical knowledge to realistically constrain such models. However, if we ap-
331 proach this problem with Occam's razor with respect to the mechanism of plasticity we arrive at a model in which the
332 global potentiation of GABAergic synapses drives habituation. Potentiation of GABAergic output through inhibitory
333 long-term potentiation (i-LTP) could explain why GABAergic neurons do not potentiate in their firing pattern, but still
334 exhibit increasing influence over the circuit during habituation. Assuming that excitatory activation in the circuit is
335 consistent, differential connectivity weights between GABAergic neurons and the other neuronal classes could drive
336 the differential rates of depression: i-LTP at strong GABAergic connections drives strong depression, while i-LTP at
337 weak GABAergic connections drives weak depression (*Figure 8A, Model 2*).

338 To test this model, we asked how PTX and Melatonin influence the dynamic activity states in different classes
339 of neurons. Antagonism of GABA receptors via PTX should decrease the influence of these inhibitory neurons on
340 the remaining populations, shifting the balance from strong depression towards weaker or non-adapting response
341 profiles. We have found that Melatonin potently increases habituation behaviour (*Figure 3*), and further depresses
342 brain-wide neuronal activity during habituation beyond normal levels (*Figure 4*). These are effectively opposite of the
343 effect of PTX, and thus we hypothesized that Melatonin acts in concert with GABA in the circuit, shifting the balance
344 towards strongly depressing profiles. This model of the action of Melatonin also fits with the observations that

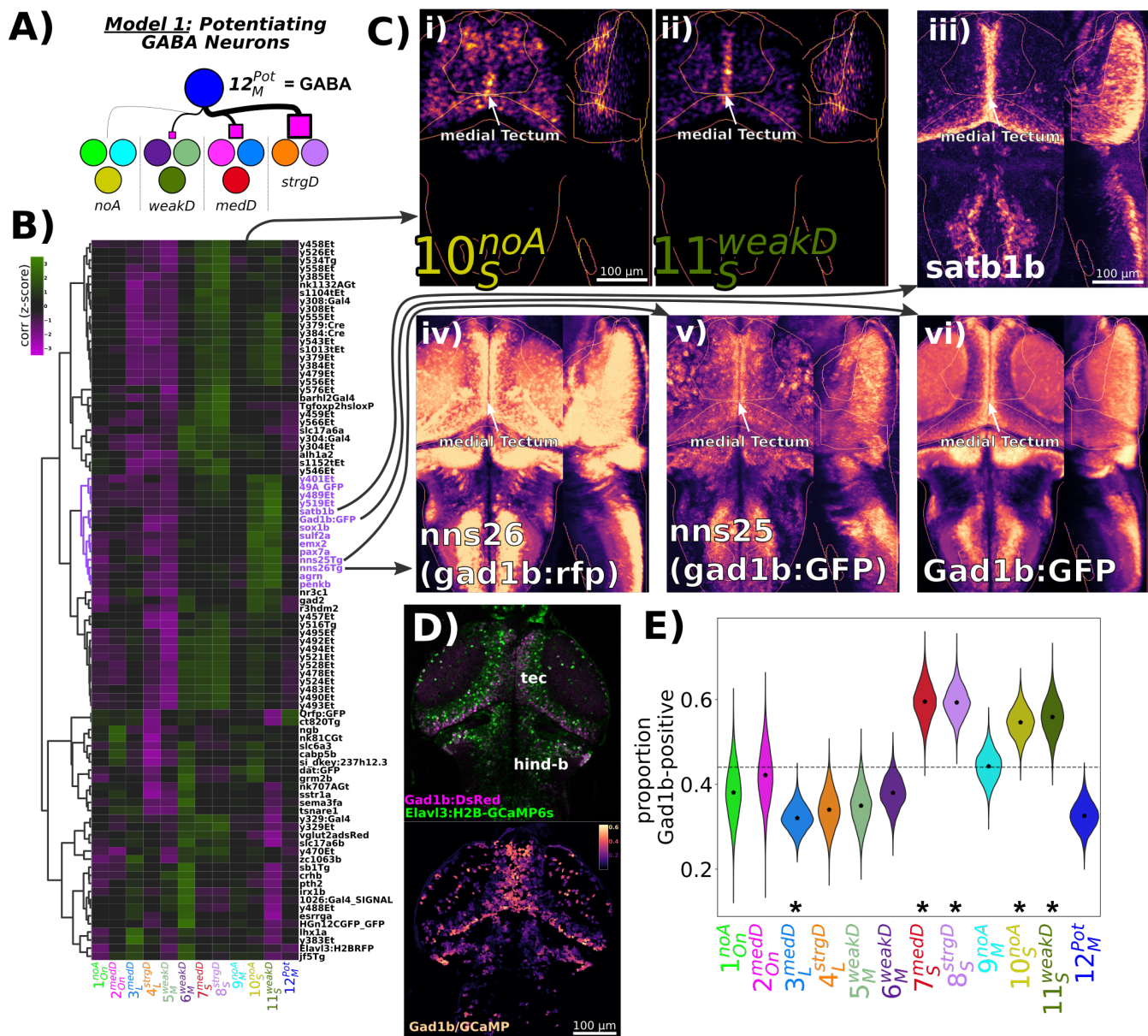


Figure 7. An atlas-based search for molecular markers identifies GABAergic neuronal classes.

A) Model 1, proposed to explain how potentiating GABAergic inhibition could mediate the range of depressive adaptations observed during habituation. Model posits that the sensitizing neurons are GABAergic (12_{M}^{Pot} , blue), and they differentially connect to functional subtypes: Strong connectivity to strongly habituating classes, weak connectivity to weakly habituating classes, etc.

B) Hierarchically clustered heatmap depicting the correlation of markers aligned to the Z-Brain atlas with the spatial arrangement of the 12 functional clusters (distance = complete, correlation). Correlation values are z-scored by rows to highlight the cluster(s) most strongly correlated or anti-correlated with a given marker. The subset of the hierarchy containing the *gad1b*-reporters is coloured in purple.

C) Normalized summed intensity projections comparing the spatial arrangements of i) 10_{S}^{noA} , and ii) 11_{S}^{weakD} with atlas markers found within the purple cluster iii) *satb1b* HCR (Shainer et al., 2022), mapZebrain Atlas iv) *nns25*, aka *TgBAC(gad1b:RFP)* (Satou et al., 2013), mapZebrain Atlas v) *nns26*, aka *TgBAC(gad1b:LOXP-RFP-LOXP-GFP)* (Satou et al., 2013), mapZebrain Atlas vi) *TgBAC(gad1b:GFP)* (Satou et al., 2013), Z-Brain Atlas

D) 2-photon imaging of *Tg(Gad1b:DsRed);Tg(elavl3:H2B-GCaMP6s)* larvae depicting the raw data for each channel (top), and the ratio of Gad1b/GCaMP6s fluorescence in each ROI functionally identified using suite2p.

E) ROIs imaged in double transgenic larvae are assigned a cluster identity based on their correlation to the cluster mean trace, and classified as Gad1b-positive based on a DsRed/GCaMP6s ratio of greater than 0.25. Dotted line = expected proportion based on total number of cells classified as Gad1b-positive. * $p < 0.05$, Chi Square test with Bonferroni correction. Distributions underlying violin plots calculated by bootstrapping 5000 replicates. $n = 1835$ ROIs in 6 larvae.

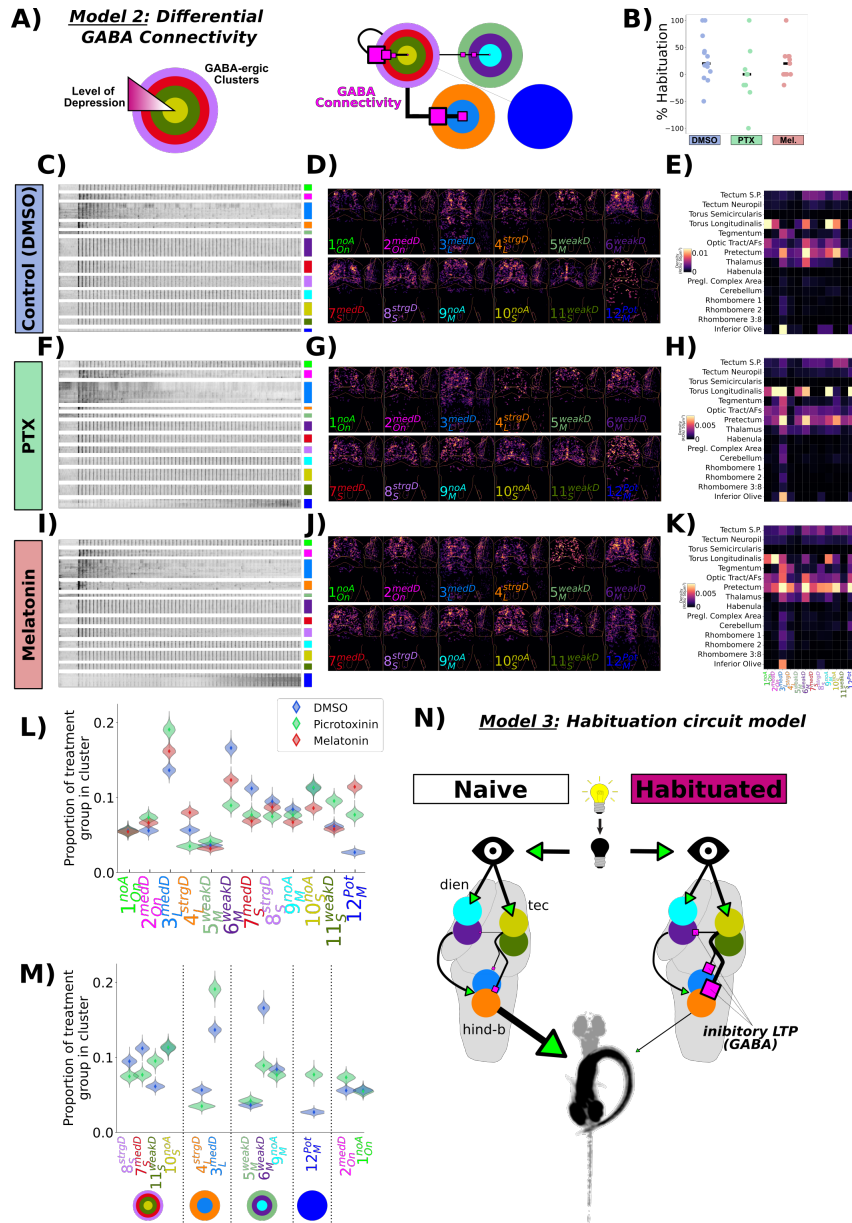


Figure 8. A pharmacologically constrained model for dark flash habituation

A) Model 2, proposed to explain how biased GABAergic inhibition could mediate the differential habituation rates observed across functional classes of neurons. Model proposes that the neurons with the Sort Response Shape are GABAergic, and that they differentially connect to the other functional subtypes, as well as themselves to drive the response decreases observed during habituation. The strength of this inhibitory connectivity determines the decrease in responsiveness across neuronal classes. Larger pink box = Stronger inhibition.

$$\text{Percent Habituation} = 100 \times (1 - \frac{P(\text{Resp}_{31-60})}{0.5 \times (P(\text{Resp}_{1-30}) + P(\text{Resp}_{31-60}))})$$

C-K) Functional clustering of neurons from larvae treated with DMSO (vehicle control), Picrotoxinin (PTX, 10 μ M), or Melatonin (1 μ M). C,F,I) Heatmap of response profiles of ROIs categorized into the 12 functional clusters. D,G,J) Summed intensity projection of the ROIs belonging to each functional cluster in Z-Brain coordinate space depicting their physical locations in the brain. Projection images are normalized to the maximum value. E,H,K) Heatmap depicting the density of each cluster that is found within different Z-Brain regions. C-E) DMSO, n = 428,720 total ROIs in 14 larvae F-H) Picrotoxinin (PTX), n = 271,037 total ROIs in 9 larvae I-K) Melatonin treatment, n = 350,516 total ROIs in 11 larvae. **L)** Proportion of neurons belonging to each functional cluster across treatment groups. Distributions for violin plots are bootstrapped from 5000 replicates.

M) Same data as M, only showing the data for PTX vs DMSO vehicle control, re-ordered to reflect the cluster Adaptation Profiles.

N) Model 3, proposed circuit model for the habituation of the probability of responding to a DF stimulus. The dark flash stimulus is detected by the retina and sent as an unadapted signal to the brain. GABA-ergic inhibitory neurons form the critical node in the habituating circuit, where habituation occurs as the result of a potentiation of GABAergic synapses, resulting in depressed responses in connected neurons. The strength of neuronal adaptation during habituation depends on the GABAergic connectivity strength (as in Model 2 (A)). The output neurons of the circuit are the Long-responding class. Potentiated GABAergic inhibition onto this population silences behavioural output.

Figure 8—figure supplement 1. Mean response of functionally identified clusters after different pharmacological treatments

345 Melatonin can directly potentiate the effects of GABA *Cheng et al. (2012); Niles et al. (1987)*. Alternatively Melatonin
346 may signal through one of 6 known G-protein coupled receptors in larval zebrafish *Maugars et al. (2020)*, which
347 could act to modulate activity states in GABAergic neurons or their targets.

348 We compared the Ca²⁺ activity patterns in neurons from fish treated with vehicle (0.1% DMSO), PTX, or Melatonin
349 (*Figure 8B-M*). At the behavioural level, we found a trend indicating that we were able manipulate habituation phar-
350 macologically in our tethered imaging assay, though this was very subtle (*Figure 8B*). This discrepancy relative to the
351 very strong behavioural effects in freely-swimming animals (*Figure 3*) likely result from the head-restrained proto-
352 col, which itself strongly inhibits behavioural output. Therefore assaying for habituation at the behavioural level is
353 difficult to interpret. Alternatively, drug access to the brain may have been compromised by the agarose mounting
354 resulting in weaker behavioural effects. Yet, since we did observe a trend in behavioural data, we proceeded under
355 the assumption that the drugs were having the desired effects.

356 We examined the activity profiles of neurons that belonged to the 12 different functional clusters. Surprisingly,
357 we observed no strong alterations of the response profiles of these neurons (*Figure 8C-K, Figure 8-figure Supple-*
358 *ment 1*). However, what was clearly altered was the proportion of neurons that belonged to different functional
359 classes (*Figure 8L,M*).

360 From these analyses we conclude the following:

- 361 **A)** The pharmacological manipulations did not alter the activity of neurons in such a way as to alter the average
362 activity states of the population within each cluster (*Figure 8-figure Supplement 1*). Instead, the proportion
363 of neurons belonging to different functional classes changed. This may result from our classification scheme,
364 or could point to fixed and relatively inflexible processing strategies that the brain is using in the context of
365 dark-flash habituation.
- 366 **B)** The effect of PTX on cluster reassignment generally followed the type of effects predicted from Model 2, in-
367 creasing the proportion of cells falling into the weaker depressing classes (*Figure 8M*). This pattern was most
368 clear in the classes with "Short" and "Long" *Response Shapes*, which are those that included the most strongly
369 depressed classes of neurons, and would thus be the most influenced by GABA-mediated inhibition. Non-
370 depressing classes were not strongly modulated, consistent with a model that these neurons receive little
371 GABAergic input. Therefore, we conclude that Model 2 is consistent with much, but not all of the alternations
372 in response to PTX. For example, PTX increased the proportion of 6_M^{weakD} neurons, which does not follow from
373 Model 2.
- 374 **C)** Based on our hypothesis that the effect of Melatonin is to potentiate GABAergic inhibition, we expected PTX
375 and Melatonin to have opposite effects. Similar to (B), this hypothesis is not fully supported by all of the data,
376 but is consistent with the observations in a subset of functional classes, perhaps those that are most critical
377 for the habituation of response probability. Indeed, the expected opposite effects of PTX and Melatonin were
378 present in two of the most conspicuous functional classes: 4_L^{strgD} , which is most strongly correlated with motor
379 output and thus is most closely associated with behavioural initiation (*Figure 6F*), and 11_S^{weakD} , which showed
380 the clearest GABA-like anatomical pattern in the tectum.
- 381 **D)** One of the most interesting classes of neurons we observed during habituation are those that potentiate their
382 responses (12_M^{Pot}). Remarkably, both Melatonin and PTX increased the proportion of neurons within this class.
383 This result, combined with our observation that these cells are non-GABAergic (*Figure 7E*), strongly suggests
384 that the role of these cells is not simply to suppress activity in the circuit to inhibit behavioural responses
385 (as in Model 1). The functional role played by this class of neurons during habituation remains mysterious.
386 However, it may relate to some of the common behavioural effects of Melatonin and PTX, such as the inhibition
387 of habituation when measuring response Displacement (*Figure 3A,B, Figure 3-figure Supplement 1E, F*).

388 Based on these data we propose a working model of the dark flash habituation circuit, particularly focused on
389 the elements we have implicated in the decreasing probability of response (*Figure 8N, Model 3*). At the center are
390 the GABAergic synapses, whose progressive potentiation drives habituation. Their influence on the depression of
391 excitatory neurons in the circuit is biased based on their connectivity weights, where strong connectivity drives
392 strong-habituation. Silencing of the long-responding motor-related neurons (4_L^{strgD}) suppresses O-bend responses.
393 PTX acts upon the outputs of the GABAergic neurons to decrease their influence in the circuit, thus inhibiting habit-
394 uation. Melatonin acts either by directly potentiating the action of GABA at the synapse (Cheng et al., 2012; Niles et

395 al., 1987), or by decreasing the excitability of postsynaptic neurons.

396 Discussion

397 Molecular mechanisms of DF habituation

398 In the pharmaco-behavioural data resulting from our screen, we focused our analysis on those pharmacological
399 agents and pathways that strongly and relatively specifically modulated habituation when measuring response
400 probability. We found that inhibition of GABA_{A/C} Receptors using PTX reduced habituation learning. GABA is the
401 main inhibitory neurotransmitter in the zebrafish brain, and deficits in GABA signaling lead to epileptic phenotypes
402 *Baraban et al. (2005)*. We were fortunate that our screening concentration (10μM) did not induce seizures, but was
403 still sufficient to inhibit habituation. This implies that the habituation circuit is exquisitely sensitive to changes in
404 GABA signaling at levels well below the threshold required to globally change excitatory-inhibitory balances. This
405 argues for a central rather than supporting role of GABAergic inhibition in dark-flash habituation.

406 A critical role for GABA in habituation is consistent with data from *Drosophila*, where both olfactory and gustatory
407 habituation have been linked to GABAergic interneurons *Das et al. (2011); Paranjpe et al. (2012); Trisal et al. (2022)*.
408 Therefore, this circuit motif of increasing inhibition to drive habituation may be a conserved feature of habituation,
409 which would allow for a straightforward mechanism for habituation override during dis-habituation via dis-inhibition
410 *Cooke and Ramaswami (2020); Trisal et al. (2022)*.

411 Our screen also identified that neuro-hormonal signaling is critical for habituation, where Melatonin and Estro-
412 gen receptor agonists potently increase habituation learning rate. The role of Estrogens in learning and memory
413 is well established *Luine et al. (1998); Nilsson and Gustafsson (2002)*. Though its role in habituation is less well ex-
414 plored, it has previously been shown to increase memory retention for olfactory habituation in mice *Dillon et al.*
415 *(2013)*. To our knowledge, Melatonin has not previously been implicated in habituation, though it has been impli-
416 cated in other learning paradigms *El-Sherif et al. (2003); Jilg et al. (2019)*. Notably, Melatonin was shown to block
417 operant learning at night in adult zebrafish *Rawashdeh et al. (2007)*, and therefore Melatonin appears to be able to
418 both promote or inhibit plasticity in zebrafish, depending on the paradigm.

419 While Melatonin and Estrogen were not strong candidates for involvement in DF habituation plasticity before our
420 screen, their previous associations with learning and memory reinforce the idea that these molecules play critical
421 roles in plasticity processes. In support of this idea, we have previously shown that habituation is regulated in a
422 circadian-dependent manner *Randlett et al. (2019)*, and both Melatonin and Estrogen levels fluctuate across the
423 circadian cycle *Alvord et al. (2022); Gandhi et al. (2015); Zhdanova et al. (2001)*, suggesting that either or both of
424 these pathways may act to couple the circadian rhythm with learning performance.

425 Finally, approximately 2% of the US population use Melatonin as a sleep-aid *Li et al. (2022)*, and a substan-
426 tial proportion of US women take Estrogen as part of either oral contraceptives or hormone replacement therapy.
427 Therefore, understanding the roles these molecules play in neuroplasticity is a clear public health concern.

428 Circuit mechanism of DF habituation

429 Using pERK-based whole brain activity profiling, we first identified that habituation learning is associated with a
430 broad depression of neuronal activity. These data appear consistent with a model for habituation in which plasticity
431 early within the visual pathway acts as an activity bottleneck, perhaps even in the retina. However, our Ca²⁺ imaging
432 experiments identified a diverse range of neuronal *Adaptation Profiles*, including non-adapting and potentiating
433 neurons spread throughout sensory- and motor- related areas of the brain, inconsistent with such a model. Thus,
434 non-habituated signals are transmitted throughout the brain, indicating the presence of parallel processing streams
435 during habituation.

436 This is more consistent with our previous behavioural analyses of habituation, where we postulated that mul-
437 tiple plasticity loci co- exist, arranged in both parallel and series within the circuit *Randlett et al. (2019)*. Such a
438 model is further supported with brain-wide imaging data for short-term habituation to looming stimuli, where dis-
439 tributed neurons were identified that showed differential rates of habituation *Marquez-Legorreta et al. (2022)*. It is
440 important to point out that Marquez-Legorreta et al. did not observe non-adapting or potentiating neurons in their
441 experiments. This may be due to differences in analysis methods, or could highlight a difference between short-

442 and long-term habituation circuit mechanisms, the latter of which may rely on more complex circuit mechanisms
443 involving both potentiation and suppression of responses.

444 While we do not have enough anatomical data to constrain circuit connectivity models that drive DF habituation,
445 here we demonstrate the use of pharmacology, functional imaging and neurotransmitter classifications to constrain
446 our models. Specifically, pharmacology indicated a central role for GABA in habituation, and our functional imag-
447 ing highlighted a role for distinct classes of neuronal types in the DF circuit, including potentiating neurons (12_M^{Pot}).
448 Initially, this led us to propose a very simple model for habituation, where potentiating neurons are GABAergic and
449 thus progressively inhibit the circuit during learning (Model 1). However, *in silico* co-localization analyses and double
450 transgenic Ca^{2+} imaging identified 12_M^{Pot} neurons to be predominantly non-GABAergic, thereby refuting this simple
451 model. Instead, we propose that the GABAergic neurons in the circuit are characterized by their short burst of activ-
452 ity to the stimulus onset, and that the potentiation of their synapses drives habituation (Model 3, *Figure 8N*). This a
453 somewhat unexpected model, as studies of long-term synaptic plasticity (e.g. LTP and LTD) have overwhelmingly fo-
454 cused on plasticity at excitatory synapses. Although a functional link to behaviour is less well established, long-term
455 inhibitory synaptic plasticity has been well documented, including inhibitory (i)-LTP and i-LTD *Castillo et al. (2011)*.

456 A key question then is what underlies the ranges in *Adaptation Profiles* that we see in individual neurons, which
457 include non-adapting, weak-, medium-, and strong-depressing profiles. One possible model is that i-LTP is imple-
458 mented differentially, which would require a mechanism to drive differential plasticity along different places in the
459 circuit. While feasible, such a mechanism seems somewhat complex. Instead we favor a more parsimonious model
460 in which differential connectivity from inhibitory neurons underlie these dynamics: non-adapting neurons receive
461 little inhibition thus i-LTP has little effect, while strong-depressing neurons receive strong inhibitory connections
462 undergoing i-LTP (Model 2, *Figure 8A*). While this model is certainly incomplete, it provides the initial framework for
463 the circuit-wide mechanisms leading to DF habituation, and testable hypotheses as to the connectivity and functional
464 consequences of manipulations of different neuronal classes.

465 Conspicuously absent from our models are the 12_M^{Pot} neurons. Since these neurons were increased by both
466 PTX and Melatonin, they might play a complex role in habituation. How they influence the system remains to be
467 seen, but perhaps they act to reinforce activity in weakly habituating neurons. Given their location in the hindbrain
468 they may alternatively directly feed into the reticulospinal system to modulate motor commands. Also absent from
469 our current model are the classes exhibiting an On-response profile (1_{On}^{noA} and 2_{On}^{medD}). These neurons fire at the
470 ramping offset of the stimulus, making it unlikely that they play a role in aspects of acute DF behaviour. However,
471 these neurons exist in both non-adapting and depressing forms suggesting a yet unidentified role in behavioural
472 adaptation to repeated DFs.

473 Circuit loci of DF habituation

474 Where in the brain does habituation take place? Our whole-brain MAP-Mapping experiments showed that while DFs
475 activate a very distributed circuit, little activation of the telencephalon or the hypothalamus was seen, indicating that
476 these areas are not involved in the DF response or its habituation. As discussed above, our data is inconsistent with
477 a single-bottleneck model. Instead, plasticity is distributed throughout the circuit. Since PTX inhibits most aspects of
478 habituation learning (*Figure 3Ai*), these all appear to involve GABA motifs. Moreover, the different functional classes
479 of neurons are distributed through sensory- and motor-related areas of the brain, consistent with the notion that
480 habituation plasticity occurs in a very distributed manner. While distributed, there are clear associations between
481 anatomical location and functional neuron type (*Figure 6A-E*), indicating that there is some degree of regional logic
482 to the localization of *Adaptation Profiles*. For example, 5_M^{weakD} and 6_M^{weakD} are the most prevalent in the pretectum, and
483 mostly absent from the tegmentum and posterior hindbrain, whereas 3_L^{medD} and 4_L^{strgD} are numerous in tegmentum
484 and posterior hindbrain, and thus likely occupy more downstream positions in the sensori-motor circuit.

485 The tectum is one of the largest brain areas in larval zebrafish, and is directly innervated nearly all retinal ganglion
486 cells *Robles et al. (2014)*. Therefore, the tectum is a prime candidate for implementing DF habituation for anatomical
487 reasons. In further support of this notion, the neurons we have identified as GABAergic and propose to be driving
488 habituation (7_S^{medD} , 8_S^{strgD} , 10_S^{noA} and 11_S^{weakD}) are concentrated in the tectum (*Figure 6C,D*). The tectum contains multiple
489 anatomically distinct types of GABAergic neurons, most of which are locally projecting interneurons (SINs, ITNs,
490 PVINs), although GABAergic projection neurons have been observed with axons projecting to the anterior hindbrain
491 *Gebhardt et al. (2019); Martin et al. (2022); Nevin et al. (2010); Robles et al. (2011)*. Therefore, we expect that

492 our GABAergic classes correspond to subsets of these GABAergic tectal neurons, which is testable using genetic
493 approaches based on marker co-expression and/or single cell morphometric and transcriptomic analyses.

494 Beyond the tectum, conspicuous neuronal clustering was observed in the inferior olive and cerebellum, which
495 have been implicated in motor-related learning behaviours in larval zebrafish *Ahrens et al. (2012); Lin et al. (2020);*
496 *Markov et al. (2021)*. Both structures contained many stimulus-tuned neurons (*Figure 5F*), and non-adapting (1_{On}^{noA} ,
497 9_M^{noA} and 10_S^{noA}), and potentiating (12_M^{Pot}) neurons were among the most concentrated in the cerebellum (*Figure 6C,D*).
498 Non-adapting 9_M^{noA} neurons were also prominent in the torus longitudinalis, which also contains high concentrations
499 of on-responding 1_{On}^{noA} , 2_{On}^{medD} neurons. The torus longitudinalis has recently been implicated in the binocular integration
500 of luminance cues *Tesmer et al. (2022)*, and therefore is ideally placed to influence habituation to whole-field
501 stimuli like DFs.

502 Collectively, our brain-wide imaging data point to a central role for inhibitory neurons in the tectum in habituation,
503 but also clearly implicate other brain areas, and therefore a comprehensive model will need to span many
504 regions of the brain in order to explain the neural and behavioural dynamics underlying habituation learning.

505 Conclusion

506 Habituation is the simplest form of learning, yet despite its presumed simplicity a model of how this process is
507 regulated in the vertebrate brain is still emerging. Here we have combined two powerful methods offered by the
508 larval zebrafish model: high-throughput behavioural screening and whole brain functional imaging. By applying
509 these methods to long-term habituation, we identified dozens of pharmacological agents that strongly modulate
510 habituation learning and distinct classes of neurons that are activated by DFs and are modulated during learning.
511 The systematic datasets we generated contain large amounts of additional information that await future validation
512 and integration into a unified model for DF habituation. Nonetheless they yielded a multitude of hypotheses as to
513 the molecular and circuit mechanisms of habituation that can be followed up in future studies.

514 Our approach validates the utility of virtual anatomical analyses using atlases and pharmacological manipulations
515 to test and constrain neural circuit models in pan-neuronal imaging experiments, for which anatomical and
516 molecular information is often sparse. From these analyses we have arrived at the first iteration of a brain-wide
517 circuit model for long-term dark flash habituation. We previously showed that habituation is a deceptively complex
518 phenomenon, where distributed plasticity mechanisms mediate the independent adaptation of different components
519 of responses *Randlett et al. (2019)*. The diversity of molecular pathways and functional neuronal types we
520 have identified here are consistent with that view of habituation, and indicate that considerable biological complexity
521 exists that awaits discovery within the “simplest” form of learning.

522 Methods

523 Animals

524 All experiments were performed on larval zebrafish at 5 days post fertilization (dpf), raised at a density of ≈ 1 larva/ml of E3 media in a 14:10h light/dark cycle at 28-29°C. Wild type zebrafish were of the TLF strain (ZDB-GENO-
525 990623-2). Transgenic larvae used were of the following genotypes: *Tg(elavl3:H2B-GCaMP7f)j^{j90}* *Yang et al. (2021)*,
526 *Tg(elavl3:H2B-GCaMP6s)j^{j5}* *Freeman et al. (2014)*, and *Tg(gad1b:DsRed)nns26* *Satou et al. (2013)*. Zebrafish were housed,
527 cared for, and bred at the Harvard MCB, UPenn CDB, and Lyon PRECI zebrafish facilities. All experiments were
528 done in accordance with relevant approval from local ethical committees at Harvard University, the University of
529 Pennsylvania, and the University of Lyon.

531 High-throughput screening setup

532 Larvae were assayed for behaviour in 300-well plates using the apparatus described previously *Randlett et al. (2019)*.
533 Briefly, each well is 8mm in diameter and 6mm deep, yielding a water volume of $\approx 300\mu L$. Behaviour was tracked
534 using a Mikrotron CXP-4 camera, Bitflow CTN-CX4 frame grabber, illuminated with IR LEDs (TSHF5410, digikey.com).
535 Visual stimuli were delivered via a ring of 155 WS2812B RGB LEDs (144LED/M, aliexpress.com). For a dark flash
536 stimulus, the LEDs were turned off for 1s, and then the light intensity was increased linearly to the original brightness
537 over 20s. The optomotor response was induced by illuminating every 8th LED along the top and bottom of the plate,
538 and progressively shifting the illuminated LED down the strip resulting in an approximately sinusoidal stimulus, 5.5

539 cm peak to peak, translating at 5.5 cm per second. Direction of motion was switched every 30 s, for a total testing
540 period of 1 hour, and performance was scored as the average change in heading direction towards the direction of
541 motion during these 30s epochs. Acoustic tap stimuli were delivered using a Solenoid (ROB-10391, Sparkfun). The
542 behavioural paradigm was designed to be symmetrical such that 1hr worth of stimulation was followed by 1hr worth
543 of rest (*Figure 1B*), allowing us to alternate the view of the camera between two plates using 45-degree incidence
544 hot mirrors (43-958, Edmund Optics) mounted on stepper motors (*Figure 1A*, ROB-09238, Sparkfun), driven by an
545 EasyDriver (ROB-12779, Sparkfun).

546 Apparatus were controlled using arduino microcontrollers (Teensy 2.0 and 3.2, PJRC) interfaced with custom
547 written software (Multi-Fish-Tracker), available here:
548 github.com/haesemeyer/MultiTracker.

549 **Behavioural analyses**

550 The behaviour of the fish was tracked online at 28 hz, and 1-second long videos at 560 hz were recorded in response
551 to DF and Acoustic Tap stimuli. Offline tracking on recorded videos was performed in MATLAB (Mathworks) using the
552 script ‘TrackMultiTrackerTiffStacks_ParallelOnFrames.m’, as described previously, to track larval posture *Randlett*
553 *et al.* (2019). Tracks were then analyzed using Python. Analysis code available here:
554 github.com/owenrandlett/lamire_2022.

555 Responses to DFs and to taps were identified as movement events that had a bend amplitude greater than
556 3rad and 1rad , respectively. Behavioural fingerprints were created by first calculating the average value for each
557 fish reflecting either the DF response during the specified time period (Naive = DFs 1-5, Training = DFs 6-240, Test
558 = DFs 241-300), or the average response during the entire stimulus period (Acoustic Taps, OMR, Free Swimming).
559 Periods where the tracking data was incomplete were excluded from the analysis. DFs where larvae did not respond
560 were excluded from the behavioural components other than the Probability of Response. The Strictly Standardized
561 Mean Difference was then calculated for each of these average fish values for the drug treated larvae DMSO control
562 (*Figure 1C*). The threshold for determining hit compounds was set at $|SSMD| \geq 2$. These analyses were performed
563 using:

564 [Analyze_MultiTracker_TwoMeasures.py](https://github.com/owenrandlett/Analyze_MultiTracker_TwoMeasures.py).

565 Hierarchical clustering (*Figure 1D*, 2A-C) was performed using SciPy *Virtanen et al.* (2020). Correlations across
566 different behavioural measures (*Figure 2D*) was calculated computing all pairwise comparisons for each behavioural
567 measure in the SSMD fingerprint across the 176 hit compounds.

568 Further details and code for the analyses used to create the figure panels are in the following notebook:
569 [2022_LamireEtAl_BehavFigs.ipynb](https://github.com/owenrandlett/2022_LamireEtAl_BehavFigs.ipynb). Analyses made use of open-source Python packages, including: NumPy *Harris*
570 *et al.* (2020), SciPy *Virtanen et al.* (2020), matplotlib *Hunter* (2007), seaborn *Waskom* (2021), and open-cv *Bradski*
571 (2000).

572 **Pharmacology**

573 Compounds were prepared as 1000x frozen stock solutions in DMSO. Stock solutions were initially diluted 1:100
574 in E3, yielding a 10x solution. 30 μL of this solution was then pipetted into the wells, yielding a 1x drug solution
575 in 0.1% DMSO (Sigma). Vehicle treatment followed the same protocol, using pure DMSO. The drug library (Sell-
576 eckchem Bioactive: 2100 FDA-approved/FDA-like small molecules, *Figure 1-source data 1*) was obtained from the
577 UPenn High-Throughput Screening Core. The library concentration was 10mM, and thus all drugs were screened at
578 approximately 10 μM .

579 For subsequent pharmacological experiments chemicals were obtained from: Picrotoxinin: Sigma, P-8390; Melan-
580 tonin: Cayman, 14427; Sigma, M5250; Ethinyl Estradiol: Cayman, 10006486; Hexestrol: Sigma, H7753

581 **MAP-Mapping**

582 Immunostaining was performed as previously described *Randlett et al.* (2015), on wild type zebrafish bleached
583 with 1.5% H_2O_2 , 1% KOH. Confocal stacks were aligned to the Z-Brain atlas coordinates using the computational
584 morphometry toolkit (CMTK, nitrc.org/projects/cmtk/), and calculations of the pairwise differences in pERK/tERK
585 staining were performed as described in, code available here:
586 github.com/owenrandlett/Z-Brain.

587 Regional analyses (*Figure 4*A-K(insets), L, M) were performed on regions of the brain as defined by the updated
588 MECE (Mutually Exclusive, Collectively Exhaustive) regional definitions, which unambiguously assign each voxel in
589 the Z-Brain to a single region arranged in a hierarchical ontology (Vorha et al, unpublished) ; available here:
590 <https://zebrafishatlas.zib.de/lm>

591 **Microscopy**

592 Imaging was performed on 5dpf larvae, mounted tail-free in 2% LMP agarose (Sigma A9414) in E3, using a 20x 1.0NA
593 water dipping objective (Olympus). Volumetric Imaging (*Figure 5*,*Figure 6*, *Figure 8*) was performed at 930 nm on a
594 Bruker Ultima microscope at the , using a resonant scanner resonant scanner over a rectangular region of 1024x512
595 pixels (0.6 μ m x/y resolution) and piezo objective mount for fast z-scanning. Imaging sessions began by taking an
596 “Anatomy Stack” consisting of 150 slices at 1 μ m z-steps, summed over 128 repeats (imaging time \approx 11 minutes). This
597 served as the reference stack used for alignment to the Z-Brain atlas, and to detect Z-drift in the imaging session
598 (see below). The functional stack consisted of 12 slices separated at 10 μ m steps, thus covering 120 μ m in the brain
599 acquired at 1.98 hz). To image *Tg(elavl3:H2B-GCaMP6s);Tg(gad1b:DsRed)* double transgenic larvae (*Figure 7*), we used
600 a custom built 2-photon microscope *Haesemeyer et al. (2018)*, imaging 512x512 images at (0.98 μ m x/y resolution) at
601 1.05 hz. The anatomy stack was taken at 2 μ m step sizes for both the green and red channels in the dark. Functional
602 imaging was performed only on the green/GCaMP channel since the red stimulus LED was incompatible with DsRed
603 imaging.

604 When developing this protocol we determined that substantial shifts of more than a cell-body diameter (5 μ M) in
605 the Z-plane are common during the \approx 1.2 hrs of imaging. We determined this by comparing the sum of the functional
606 image planes during 5 equally sized time epochs (1540 frames per epoch), aligned to the “Anatomy Stack”, using
607 “phase_cross_correlation” in the scikit-image library *van der Walt et al. (2014)*. This allowed us to quantify shifts in
608 the imaging plane as shifts in this alignment. These tended to occur within the first hour of imaging, therefore we
609 performed an hour of imaging of this functional stack before beginning the DF stimulation protocol to allow the
610 preparation to settle under imaging conditions. Dark flashes were delivered using a 3mm red LED mounted above
611 the fish, controlled by an Arduino Nano connected to the microscope GPIO board and the Prairie View software to
612 deliver pulses of darkness consisting of 1 sec light off, 20 sec linear ramp back to light on, delivered at 60 second
613 intervals.

614 Even with this pre-imaging protocol, z-shifts were still observed in a considerable number of fish. Since our
615 habituation-based analysis is focused on how individual neurons change their responses over time, shifts in the
616 z-plane are extremely problematic as they are not correctable post-acquisition and can result in different neurons
617 being imaged at individual voxels. This could easily be confused for changes in functional responses over time during
618 habituation. Therefore, any fish showing a z-drift of greater than 3 μ m was excluded from our analysis. Stable z-
619 positioning was further confirmed by manual inspection of the eigan images in the imaging timecourse using “View
620 registration metrics” in suite2 to confirm that these do not reflect z-drift. Of 56 larvae imaged total, 22 were
621 excluded, leaving 34 included. Larvae were treated with 0.1% DMSO, Picrotoxinin (PTX, 10 μ M), or Melatonin (1 μ M),
622 from approximately 1hr before imaging. These fish were analyzed as a single population (*Figure 5*,*Figure 6*,*Figure 7*)
623 and separately to determine the effects of the treatments (*Figure 8*).

624 **Ca²⁺ imaging analysis**

625 ROIs were identified using suite2p *Pachitariu et al. (2017)* using the parameters outlined in
626 RunSuite2p_BrukerData_ScreenPaper.py and RunSuite2p_MartinPhotonData_ScreenPaper.py scripts for the data
627 from the Bruker Ultima microscope (*Figure 5*-*Figure 8*), and custom built 2-photon microscope (*Figure 7*D,E), respec-
628 tively. These ROIs mostly reflected individual neuronal nuclei/soma. The imaging planes were then aligned to the
629 anatomical stack taken before functional imaging using “phase_cross_correlation” in the scikit-image library *van der*
630 *Walt et al. (2014)*. For the volumetric data, the anatomical stack was then aligned to the Z-Brain atlas coordinates
631 using CMTK, and ROI coordinates were transformed into Z-Brain coordinates using streamxform in CMTK. These
632 steps were performed using
633 ??Bruker2p_AnalyzePlanesAndRegister.py.

634 To identify ROIs that were correlated with the stimulus we use a regression-based approach *Miri et al. (2011)*,
635 where we identified ROIs that were correlated with vectors representing the time course of the DF stimuli convolved

636 with a kernel approximating the slowed H2B-GCaMP time course with respect to neuronal activity. These regressors
637 reflected either the entire 21 second dark flash stimulus, or only the onset of the flash, and either the first 3, last 3,
638 or all 60 flashes (6 regressors in total). To identify neurons correlated to motor output, we took advantage of the
639 plane-based registration statistics calculated by suite2p. Specifically, the “ops[‘corrXY’]” metric, which reflects the
640 correlation of each registered image frame with the reference image. We reasoned that movements would cause
641 image artifacts and distortions that would be reflected as a transient drop in these correlations. Indeed, we con-
642 firmed this association by imaging the tail using an infrared camera, and compared the motion index calculated
643 through tail tracking, and that which we calculated based on the motion artifacts, which showed good overall agree-
644 ment in predicted movement events and average correlation of 0.4, demonstrating that these image-based artifacts
645 can be used as reliable proxies of tail movements (*Figure 5-figure Supplement 1*). Therefore, regressors based on
646 these motion indices were used to identify neurons correlated with motor output.

647 Images for the functional tuning of individual neurons (*Figure 5E-H*) were computed using the the Hue Saturation
648 Value (HSV) colorscheme, with the maximal correlation value to either regressor mapped to saturation, and the
649 hue value reflecting the linear preference for either regressor. Clustering of functional response types (*Figure 6*)
650 was done by first selecting all those ROIs that showed a correlation of 0.25 or greater with any of the 6 stimulus
651 regressors across all imaged fish. Then among these ROIs we removed any ROIs that did not show a correlation of
652 0.3 or greater with at least 5 ROIs imaged in a different larvae. This filtered out ROIs that were unique in any individual
653 fish, allowing us to focus on those neuron types that were most consistent across individuals. We then used the
654 Affinity Propagation clustering from scikit-learn *Pedregosa et al. (2011)*, with “affinity” computed as the Pearson
655 product-moment correlation coefficients (corrcoef in NumPy *Harris et al. (2020)*), preference=-9, and damping=0.9.

656 To generate the final cluster assignments we re-scanned all the ROIs calculating their correlation with the mean-
657 response vectors for each of the identified 12 functional clusters, selecting those with a correlation value of 0.3 or
658 greater, which were then assigned to the cluster with which they had the highest correlation. To determine the clus-
659 ter assignments for the data from *Tg(Gad1b:DsRed);Tg(elavl3:H2B-GCaMP6s)* double transgenic larvae (*Figure 7D,E*)
660 data were realigned and interpolated to match the frame rate of the clustered data, and assigned to the 12 clusters
661 as above.

662 To compare the spatial relationships between the neuronal positions of different clusters (*Figure 6E*), and be-
663 tween the clusters and reference brain labels (*Figure 7B,C*), image volumes were cropped to the imaged coordi-
664 nates (*Figure 5C*), downsampled to isometric 10 μm^3 voxels, and linearized to calculate the Pearson’s correlation
665 coefficient between the image sub-volumes.

666 Analyses made use of multiple open-source Python packages, including: suite2p *Pachitariu et al. (2017)* NumPy
667 *Harris et al. (2020)*, SciPy *Virtanen et al. (2020)*, scikit-learn *Pedregosa et al. (2011)*, scikit-image *van der Walt et al.*
668 (*2014*), numba *Lam et al. (2015)*, matplotlib *Hunter (2007)*, seaborn *Waskom (2021)*, and open-cv *Bradski (2000)*.
669 Details of the analyses used to create the figure panels are in the following notebook:
670 [2022_LamireEtAl_FunctionalFigs.ipynb](#)

671 Data and Code Availability

672 Code for data analysis and for generating the figure panels is available here:

673 github.com/owenrandlett/lamire_2022

674 Data are available here:

675 lamire2022.randlettlab.com/

676 Acknowledgments

677 We thank the Randlett, Granato and Engert group members for helpful advice regarding the manuscript and work,
678 Gregory Forkin for help in zebrafish husbandry, and the Burgess and Baier groups for sharing anatomical data from
679 the Zebrafish Brain Browser and mapZebrain atlases. This work was supported by funding from the ATIP-Avenir
680 program of the CNRS and Inserm (O.R.), a Fondation Fyssen research grant (O.R.), the IDEX-Impulsion initiative of
681 the University of Lyon (O.R.), the NIH RO1 grant MH109498 (M.G.) and the NIH Brain Initiative grants U19NS104653,
682 R24 NS086601, and R43OD024879, as well as Simons Foundation grants SCGB nos. 542973 and 325207 (F.E.)

683 Author Contributions

684 Conceptualization: OR, MG
685 Methodology: OR
686 Software: OR, MH
687 Formal Analysis: OR
688 Investigation: L-AL, OR
689 Supervision, Resources and Funding Acquisition: FE, MG, OR
690 Writing – Original Draft Preparation: OR
691 Writing – Review Editing: MH, FE, MG, LA-L, OR
692

693 References

- 694 Ahrens MB, Li JM, Orger MB, Robson DN, Schier AF, Engert F, Portugues R. Brain-wide neuronal dynamics during motor adaptation
695 in zebrafish. *Nature*. 2012 May; 485(7399):471–477.
- 696 Alvord VM, Kantra EJ, Pendergast JS. Estrogens and the circadian system. *Semin Cell Dev Biol*. 2022 Jun; 126:56–65.
- 697 Bailey CH, Chen M. Morphological basis of long-term habituation and sensitization in Aplysia. *Science*. 1983 Apr; 220(4592):91–93.
- 698 Bandara SB, Carty DR, Singh V, Harvey DJ, Vasylyeva N, Pressly B, Wulff H, Lein PJ. Susceptibility of larval zebrafish to the seizurogenic
699 activity of GABA type A receptor antagonists. *Neurotoxicology*. 2020 Jan; 76:220–234.
- 700 Baraban SC, Taylor MR, Castro PA, Baier H. Pentylenetetrazole induced changes in zebrafish behavior, neural activity and c-fos
701 expression. *Neuroscience*. 2005; 131(3):759–768.
- 702 Bradski G. The openCV library. *Dr Dobb's Journal: Software Tools for the Professional Programmer*. 2000; 25(11):120–123.
- 703 Bruni G, Rennekamp AJ, Velenich A, McCarroll M, Gendelev L, Fertsch E, Taylor J, Lakhani P, Lensen D, Evron T, Lorello PJ, Huang
704 XP, Kolczewski S, Carey G, Calderone BJ, Prinssen E, Roth BL, Keiser MJ, Peterson RT, Kokel D. Zebrafish behavioral profiling
705 identifies multitarget antipsychotic-like compounds. *Nat Chem Biol*. 2016 Jul; 12(7):559–566.
- 706 Burgess HA, Granato M. Modulation of locomotor activity in larval zebrafish during light adaptation. *J Exp Biol*. 2007 Jul; 210(Pt
707 14):2526–2539.
- 708 Castillo PE, Chiu CQ, Carroll RC. Long-term plasticity at inhibitory synapses. *Curr Opin Neurobiol*. 2011 Apr; 21(2):328–338.
- 709 Chen X, Engert F. Navigational strategies underlying phototaxis in larval zebrafish. *Front Syst Neurosci*. 2014 Mar; 8:39.
- 710 Cheng XP, Sun H, Ye ZY, Zhou JN. Melatonin modulates the GABAergic response in cultured rat hippocampal neurons. *J Pharmacol
711 Sci*. 2012 May; 119(2):177–185.
- 712 Cooke SF, Komorowski RW, Kaplan ES, Gavornik JP, Bear MF. Visual recognition memory, manifested as long-term habituation,
713 requires synaptic plasticity in V1. *Nat Neurosci*. 2015 Feb; 18(2):262–271.
- 714 Cooke S, Ramaswami M. Ignoring the Innocuous: The Neural Mechanisms of Habituation. In: *The Cognitive Neurosciences: 6th
715 Edition* MIT Press; 2020.p. 197.
- 716 Das S, Sadanandappa MK, Dervan A, Larkin A, Lee JA, Sudhakaran IP, Priya R, Heidari R, Holohan EE, Pimentel A, Gandhi A, Ito K,
717 Sanyal S, Wang JW, Rodrigues V, Ramaswami M. Plasticity of local GABAergic interneurons drives olfactory habituation. *Proc
718 Natl Acad Sci U S A*. 2011 Sep; 108(36):E646–54.
- 719 Dillon TS, Samuel Dillon T, Fox LC, Han C, Linster C. 17β -estradiol enhances memory duration in the main olfactory bulb in CD-1
720 mice; 2013.
- 721 Dunn TW, Mu Y, Narayan S, Randlett O, Naumann EA, Yang CT, Schier AF, Freeman J, Engert F, Ahrens MB. Brain-wide mapping of
722 neural activity controlling zebrafish exploratory locomotion. *Elife*. 2016 Mar; 5:e12741.
- 723 El-Sherif Y, Tesoriero J, Hogan MV, Wierszko A. Melatonin regulates neuronal plasticity in the hippocampus. *J Neurosci Res*. 2003;
724 72(4):454–460.
- 725 Förster D, Helmbrecht TO, Mearns DS, Jordan L, Mokayes N, Baier H. Retinotectal circuitry of larval zebrafish is adapted to detection
726 and pursuit of prey; 2020.

- 727 **Freeman J**, Vladimirov N, Kawashima T, Mu Y, Sofroniew NJ, Bennett DV, Rosen J, Yang CT, Looger LL, Ahrens MB. Mapping brain
728 activity at scale with cluster computing. *Nat Methods*. 2014 Sep; 11(9):941–950.
- 729 **Gandhi AV**, Mosser EA, Oikonomou G, Prober DA. Melatonin is required for the circadian regulation of sleep. *Neuron*. 2015 Mar;
730 85(6):1193–1199.
- 731 **Gebhardt C**, Auer TO, Henriques PM, Rajan G, Durore K, Bianco IH, Del Bene F. An interhemispheric neural circuit allowing
732 binocular integration in the optic tectum. *Nat Commun*. 2019 Nov; 10(1):5471.
- 733 **Glanzman DL**. Habituation in Aplysia: the Cheshire cat of neurobiology. *Neurobiol Learn Mem*. 2009 Sep; 92(2):147–154.
- 734 **Gupta T**, Marquart GD, Horstick EJ, Tabor KM, Pajevic S, Burgess HA. Morphometric analysis and neuroanatomical mapping of the
735 zebrafish brain. *Methods*. 2018 Nov; 150:49–62.
- 736 **Haesemeyer M**, Robson DN, Li JM, Schier AF, Engert F. A Brain-wide Circuit Model of Heat-Evoked Swimming Behavior in Larval
737 Zebrafish. *Neuron*. 2018 May; 98(4):817–831.e6.
- 738 **Harris CR**, Millman KJ, van der Walt SJ, Gommers R, Virtanen P, Cournapeau D, Wieser E, Taylor J, Berg S, Smith NJ, Kern R, Picus M,
739 Hoyer S, van Kerkwijk MH, Brett M, Haldane A, Del Río JF, Wiebe M, Peterson P, Gérard-Marchant P, et al. Array programming
740 with NumPy. *Nature*. 2020 Sep; 585(7825):357–362.
- 741 **Hunter**. Matplotlib: A 2D Graphics Environment. . 2007 May; 9:90–95.
- 742 **Jilg A**, Bechstein P, Saade A, Dick M, Li TX, Tosini G, Rami A, Zemmar A, Stehle JH. Melatonin modulates daytime-dependent synaptic
743 plasticity and learning efficiency. *J Pineal Res*. 2019 Apr; 66(3):e12553.
- 744 **Kaplan ES**, Cooke SF, Komorowski RW, Chubykin AA, Thomazeau A, Khibnik LA, Gavornik JP, Bear MF. Contrasting roles for
745 parvalbumin-expressing inhibitory neurons in two forms of adult visual cortical plasticity. *Elife*. 2016 Mar; 5.
- 746 **Kunst M**, Laurell E, Mokayes N, Kramer A, Kubo F, Fernandes AM, Förster D, Dal Maschio M, Baier H. A Cellular-Resolution Atlas
747 of the Larval Zebrafish Brain; 2018.
- 748 **Lam SK**, Pitrou A, Seibert S. Numba: a LLVM-based Python JIT compiler. In: *Proceedings of the Second Workshop on the LLVM Compiler
749 Infrastructure in HPC* No. Article 7 in LLVM ’15, New York, NY, USA: Association for Computing Machinery; 2015. p. 1–6.
- 750 **Li J**, Somers VK, Xu H, Lopez-Jimenez F, Covassin N. Trends in Use of Melatonin Supplements Among US Adults, 1999–2018. *JAMA*.
751 2022 Feb; 327(5):483–485.
- 752 **Lin Q**, Manley J, Helmreich M, Schlumm F, Li JM, Robson DN, Engert F, Schier A, Nöbauer T, Vaziri A. Cerebellar Neurodynamics
753 Predict Decision Timing and Outcome on the Single-Trial Level. *Cell*. 2020 Jan; 0(0).
- 754 **Luine VN**, Richards ST, Wu VY, Beck KD. Estradiol enhances learning and memory in a spatial memory task and effects levels of
755 monoaminergic neurotransmitters. *Horm Behav*. 1998 Oct; 34(2):149–162.
- 756 **Markov DA**, Petrucco L, Kist AM, Portugues R. A cerebellar internal model calibrates a feedback controller involved in sensorimotor
757 control. *Nat Commun*. 2021 Nov; 12(1):6694.
- 758 **Marquart GD**, Tabor KM, Horstick EJ, Brown M, Geoca AK, Polys NF, Nogare DD, Burgess HA. High-precision registration between
759 zebrafish brain atlases using symmetric diffeomorphic normalization. *Gigascience*. 2017 Aug; 6(8):1–15.
- 760 **Marquez-Legorreta E**, Constantin L, Piber M, Favre-Bulle IA, Taylor MA, Blevins AS, Giacometto J, Bassett DS, Vanwallegem GC,
761 Scott EK. Brain-wide visual habituation networks in wild type and fmr1 zebrafish. *Nat Commun*. 2022; 13(1):1–19.
- 762 **Martin A**, Babbitt A, Pickens AG, Pickett BE, Hill JT, Suli A. Single-Cell RNA Sequencing Characterizes the Molecular Heterogeneity
763 of the Larval Zebrafish Optic Tectum. *Front Mol Neurosci*. 2022 Feb; 15:818007.
- 764 **Maugars G**, Nourizadeh-Lillabadi R, Weltzien FA, New Insights Into the Evolutionary History of Melatonin Receptors in Vertebrates,
765 With Particular Focus on Teleosts; 2020.
- 766 **McDiarmid TA**, Belmadani M, Liang J, Meili F, Mathews EA, Mullen GP, Hendi A, Wong WR, Rand JB, Mizumoto K, Haas K, Pavlidis P,
767 Rankin CH. Systematic phenomics analysis of autism-associated genes reveals parallel networks underlying reversible impairments
768 in habituation. *Proc Natl Acad Sci U S A*. 2019 Nov; .
- 769 **McDiarmid TA**, Yu AJ, Rankin CH. Habituation Is More Than Learning to Ignore: Multiple Mechanisms Serve to Facilitate Shifts in
770 Behavioral Strategy. *Bioessays*. 2019 Aug; 8:1900077.
- 771 **Miri A**, Daie K, Burdine RD, Aksay E, Tank DW. Regression-based identification of behavior-encoding neurons during large-scale
772 optical imaging of neural activity at cellular resolution. *J Neurophysiol*. 2011 Feb; 105(2):964–980.

- 773 **Nelson JC**, Shoenhard HM, Granato M. Pharmacogenetic and whole-brain activity analyses uncover integration of distinct molecular and circuit programs that drive learning; 2022.
- 775 **Nevin LM**, Robles E, Baier H, Scott EK, Focusing on optic tectum circuitry through the lens of genetics; 2010.
- 776 **Niles LP**, Pickering DS, Arciszewski MA. Effects of chronic melatonin administration on GABA and diazepam binding in rat brain. *J Neural Transm*. 1987; 70(1-2):117-124.
- 778 **Nilsson S**, Gustafsson JA. Biological role of estrogen and estrogen receptors. *Crit Rev Biochem Mol Biol*. 2002; 37(1):1-28.
- 779 **Pachitariu M**, Stringer C, Dipoppa M, Schröder S, Rossi LF, Dalgleish H, Carandini M, Harris KD. Suite2p: beyond 10,000 neurons with standard two-photon microscopy; 2017.
- 781 **Paranjpe P**, Rodrigues V, VijayRaghavan K, Ramaswami M. Gustatory habituation in *Drosophila* relies on rutabaga (adenylate cyclase)-dependent plasticity of GABAergic inhibitory neurons. *Learn Mem*. 2012 Nov; 19(12):627-635.
- 783 **Pedregosa F**, Varoquaux G, Gramfort A, Michel V, Thirion B, Grisel O, Blondel M, Prettenhofer P, Weiss R, Dubourg V, Others. Scikit-learn: Machine learning in Python. *the Journal of machine Learning research*. 2011; 12:2825-2830.
- 785 **Ramaswami M**. Network Plasticity in Adaptive Filtering and Behavioral Habituation. *Neuron*. 2014 Jun; 82(6):1216-1229.
- 786 **Randlett O**, Haesemeyer M, Forkin G, Shoenhard H, Schier AF, Engert F, Granato M. Distributed Plasticity Drives Visual Habituation Learning in Larval Zebrafish. *Curr Biol*. 2019 Apr; 29(8):1337-1345.e4.
- 788 **Randlett O**, Wee CL, Naumann EA, Nnaemeka O, Schoppik D, Fitzgerald JE, Portugues R, Lacoste AMB, Riegler C, Engert F, Schier AF. Whole-brain activity mapping onto a zebrafish brain atlas. *Nat Methods*. 2015 Sep; 12(11):1039-1046.
- 790 **Rankin CH**, Abrams T, Barry RJ, Bhatnagar S, Clayton DF, Colombo J, Coppola G, Geyer MA, Glanzman DL, Marsland S, McSweeney FK, Wilson DA, Wu CF, Thompson RF. Habituation revisited: an updated and revised description of the behavioral characteristics of habituation. *Neurobiol Learn Mem*. 2009 Sep; 92(2):135-138.
- 793 **Rawashdeh O**, de Borsetti NH, Roman G, Cahill GM. Melatonin suppresses nighttime memory formation in zebrafish. *Science*. 2007 Nov; 318(5853):1144-1146.
- 795 **Rihel J**, Prober DA, Arvanites A, Lam K, Zimmerman S, Jang S, Haggarty SJ, Kokel D, Rubin LL, Peterson RT, Schier AF. Zebrafish behavioral profiling links drugs to biological targets and rest/wake regulation. *Science*. 2010 Jan; 327(5963):348-351.
- 797 **Robles E**, Laurell E, Baier H. The retinal projectome reveals brain-area-specific visual representations generated by ganglion cell diversity. *Curr Biol*. 2014 Sep; 24(18):2085-2096.
- 799 **Robles E**, Smith SJ, Baier H. Characterization of genetically targeted neuron types in the zebrafish optic tectum. *Front Neural Circuits*. 2011 Feb; 5:1.
- 801 **Rose JK**, Kaun KR, Chen SH, Rankin CH. GLR-1, a non-NMDA glutamate receptor homolog, is critical for long-term memory in *Caenorhabditis elegans*. *J Neurosci*. 2003 Oct; 23(29):9595-9599.
- 803 **Satou C**, Kimura Y, Hirata H, Suster ML, Kawakami K, Higashijima SI. Transgenic tools to characterize neuronal properties of discrete populations of zebrafish neurons. *Development*. 2013 Sep; 140(18):3927-3931.
- 805 **Shainer I**, Kuehn E, Laurell E, Al Kassar M, Mokayes N, Sherman S, Larsch J, Kunst M, Baier H. A single-cell resolution gene expression atlas of the larval zebrafish brain; 2022.
- 807 **Tabor KM**, Marquart GD, Hurt C, Smith TS, Geoca AK, Bhandiwad AA, Subedi A, Sinclair JL, Polys NF, Burgess HA. Brain-wide cellular resolution imaging of Cre transgenic zebrafish lines for functional circuit-mapping; 2018.
- 809 **Tesmer AL**, Fields NP, Robles E. Input from torus longitudinalis drives binocularity and spatial summation in zebrafish optic tectum. *BMC Biol*. 2022 Jan; 20(1):24.
- 811 **Trisal S**, Aranha M, Chodankar A, VijayRaghavan K, Ramaswami M. A DROSOPHILA CIRCUIT FOR HABITUATION OVERRIDE. *J Neurosci*. 2022 Mar; .
- 813 **Virtanen P**, Gommers R, Oliphant TE, Haberland M, Reddy T, Cournapeau D, Burovski E, Peterson P, Weckesser W, Bright J, van der Walt SJ, Brett M, Wilson J, Millman KJ, Mayorov N, Nelson ARJ, Jones E, Kern R, Larson E, Carey CJ, et al. SciPy 1.0: fundamental algorithms for scientific computing in Python. *Nat Methods*. 2020 Mar; 17(3):261-272.
- 816 **van der Walt S**, Schönberger JL, Nunez-Iglesias J, Boulogne F, Warner JD, Yager N, Gouillart E, Yu T, scikit-image contributors. scikit-image: image processing in Python. *PeerJ*. 2014 Jun; 2:e453.

- 818 **Waskom M.** seaborn: statistical data visualization. J Open Source Softw. 2021 Apr; 6(60):3021.
- 819 **Yang E, Zwart MF, Rubinov M, James B, Wei Z, Narayan S, Vladimirov N, Mensh BD, Fitzgerald JE, Ahrens MB.** A brainstem integrator
820 for self-localization and positional homeostasis; 2021.
- 821 **Zhdanova IV, Wang SY, Leclair OU, Danilova NP.** Interactive report. Brain Res. 2001; 903:263–268.

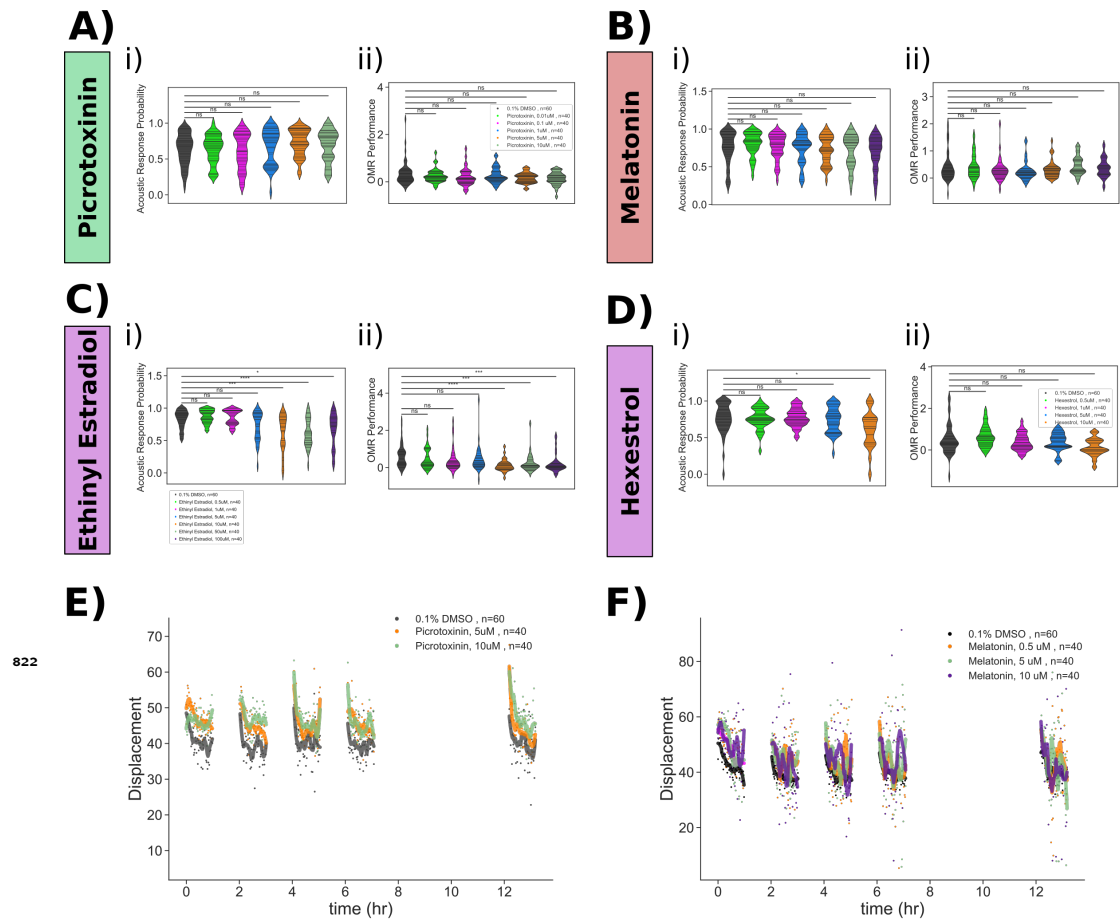


Figure 3—figure supplement 1. Pharmacological manipulation of control behaviours and response displacement during habituation.

Dose response studies for **A) Picrotoxinin**, **B) Melatonin**, **C) Ethinyl Estradiol** and **D) Hexestrol**. Displayed for each treatment are: i) Violin plots for the dose response data, showing the probability of response to 30 acoustic tap stimuli. Horizontal lines = individual fish. ii) Violin plots for the dose response data OMR performance. Horizontal lines = individual fish. Statistical tests: Mann Whitney with bonferroni correction, ns=not significant; $p \leq **** = 1 \times 10^{-4}$; *** = 1×10^{-3} ; ** = 1×10^{-2} ; * = 0.05.

E) Treatment with Picrotoxinin inhibits the decreases in movement displacement during habituation training.

F) Treatment with Melatonin inhibits the decreases in movement displacement during habituation training. Each dot is the mean response of the population to one flash. Lines are smoothed in time with a Savgolay Filter (window = 15 stimuli, order=2).

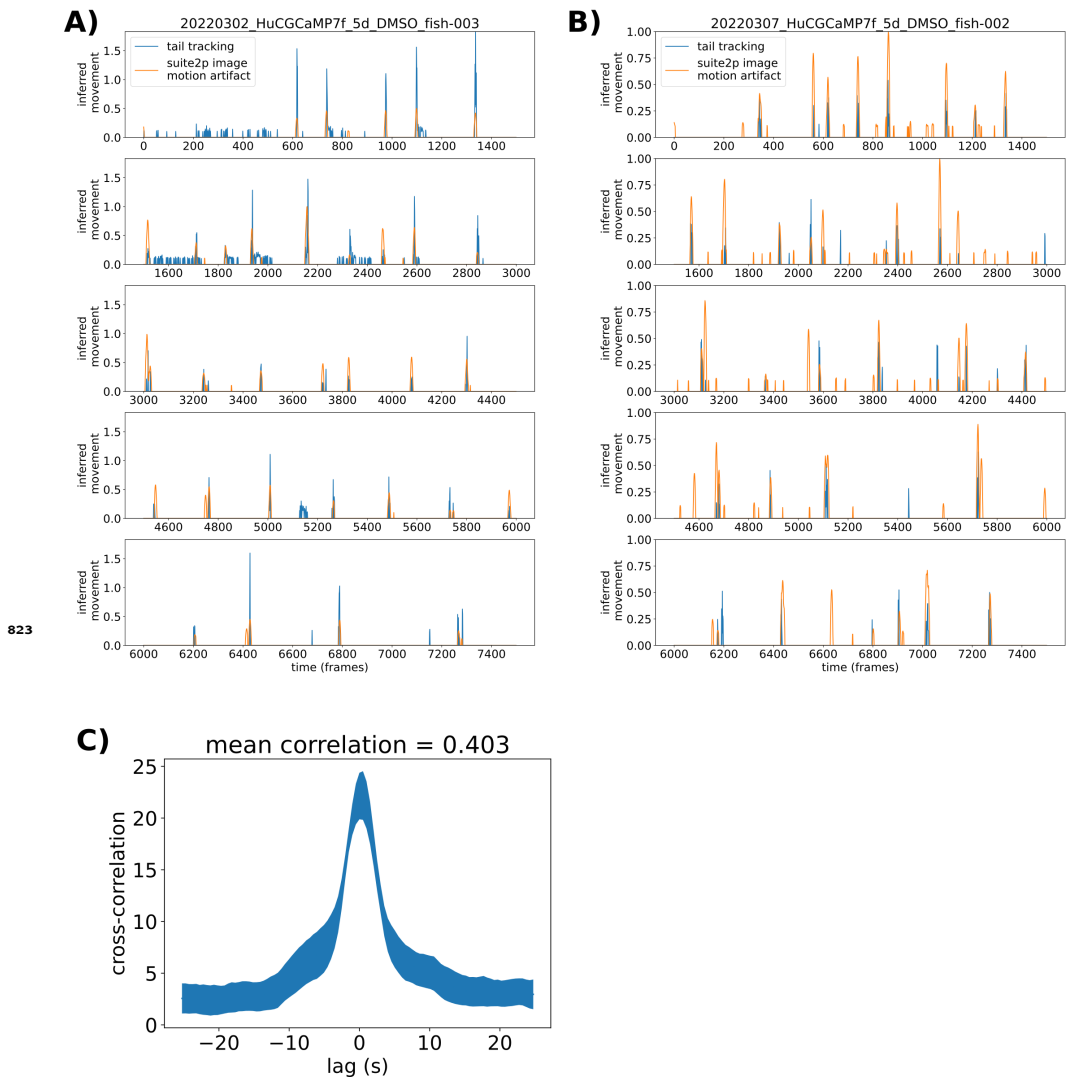


Figure 5—figure supplement 1. Validation of motion analysis based on image artifacts during 2-photon imaging.
A) Motion indexes as calculated based on tail tracking (blue) and based on decreases in the correlation between individual frames and the reference frame used for motion alignment (orange) across the entire imaging experiment (65 minutes).
B) Same analysis as (A), for a different larva.
C) Cross-correlation plot comparing the two motion index vectors. Mean across 6 larvae, and line thickness = standard error.

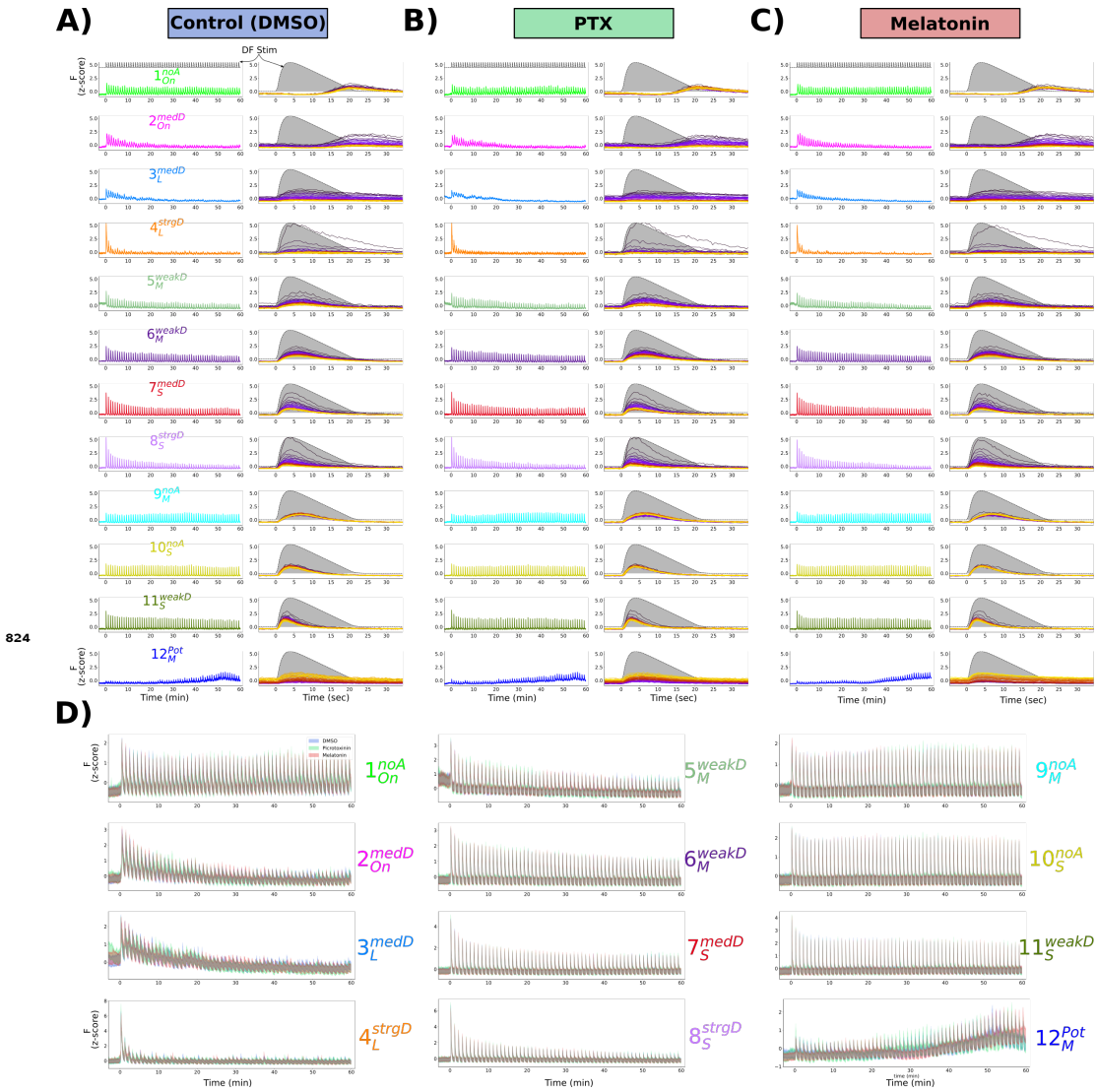


Figure 8—figure supplement 1. Mean response of functionally identified clusters after different pharmacological treatments. **A-C)** Average z-scored fluorescence each functional cluster plotted for the whole experiment (left column), and centered on each DF stimulus (right column), demonstrating the differences in both adaptation and *Response Shape* for each cluster after treatment with **(A)** 0.1% DMSO vehicle control, **(B)** Picrotoxinin (10 μ M), or **(C)** Melatonin (1 μ M). **D)** Same data as A-C, plotted together for each treatment group.